# Engineering novel endocrine nanomedicines for GBM
# Final Report

**Lead Applicant/PI**: Dr Aikaterini Lalatsa (Univ. of Portsmouth)
**Co-I**: Prof Geoff Pilkington (Univ. of Portsmouth)
**Co-I**: Prof Tim Clark (Univ. of Portsmouth/Friedrich-Alexander-Universität, Nürnberg)

## Summary

Primary brain tumours account for 12,300 new cases in the UK every year and range from the very uncommon, non-invasive, and surgically curable pilocytic astrocytomas to glioblastoma multiforme (GBM), the most common intraparenchymal brain tumour in adults, which is highly invasive and virtually incurable. Primary brain cancers grow rapidly, leading to profound morbidity and short survival. The current standard of care for newly diagnosed glioblastoma consists of maximal safe surgical resection followed by concurrent radiation therapy with temozolomide, followed by adjuvant temozolomide (Stupp protocol). This treatment resulted in an increase in median survival of 2.5 months (from 12.1 to 14.6 months) and an increase in 2-year survival of 26%. Although it is possible for some cytotoxic drugs to gain access to the major tumour mass by a virtue of damaged or incomplete blood-brain tumour barrier, such drugs fail to reach invading cancer cells which may be centimetres away from perceived edge of the tumour where the BBB is intact.

The identification of the overexpression of gonadotrophin releasing hormone (GnRH) G-protein couples receptors (GPCRs) in biopsies from GBM sufferers and the strong antiproliferative, antimetastatic, antiangiogenic dose dependent effects afforded by GnRH agonistic peptides makes them ideal novel therapies for gliomas. However, in order to develop these peptides as therapies for gliomas, they need to reach the tumour in adequate amounts, which is not possible due to their short plasma half-life (2-5 minutes) and inability to permeate biological membranes and the BBB. Even if a stable agonist is synthesised such as in the case of leuprolide and goserelin, these stable agonists are unable to cross the BBB in therapeutically relevant concentrations due to their high molecular weight and hydrophilicity. Thus, attempts to benefit from their therapeutic potential have not been achieved.

The project succeeded in provide proof-of principle for the translation of these peptide nanofibers across a range of GBM brain tumours (immortalised and low passage tumours from patient biopsies). Engineered lipidized GnRH amphiphiles produce in aqueous media stable nanofibers able to envelope clinical relevant amounts of brain impermeable chemotherapeutic drugs and target them across a range of GBM brain tumours overexpressing the GnRH receptor. Preferably, the peptide is the therapeutic and the carrier, where the cargo is loaded (or conjugated) for delivery across the BBB without requiring other excipients, polymers, or carriers. Nanofibers are stable upon dilution after intravenous administration and to enzymatic degradation, can be dose sparing for cytotoxic agents, are brain permeable, target only cells that overexpressed the receptor of interest, while they have shown excellent in vitro and acute in vivo toxicity, are formulated as a stable lyophilised powder (>2 years, -20$^{o}$C) for reconstitution prior administration, and are easily scalable and manufactured under Good Manufacturing Practice towards a Phase I trial medicine for a novel endocrine therapy for GBM patients.

### Lay Person Summary

Glioblastoma multiforme (GBM) is the most aggressive type of brain tumour with a median survival time of only 14.5 months from diagnosis to death for GBM sufferers. Despite surgical and radiotherapy advancements, one of the major problems in treating brain tumours is the inability of anti-cancer agents to enter the brain in adequate amounts and specifically target the tumour cells. This lack of accessibility of cancer cells to anti-cancer drugs is due to the protection of the brain by the blood-brain barrier (BBB), a tight membrane that separates the brain from the circulating blood and prevents 98% of all drugs from accessing the brain.

Biopsies from GBM patients have indicated the presence in higher amounts of cell membrane switches known as G-protein coupled receptors (GPCRs) on the surface of brain cancer cells than on normal cells. These switches, when turned on by specific peptides (small proteins), such as gonadotrophin releasing hormone, can inhibit the growth and spread of the cancer cells. However, these peptides cannot be used to treat GBM because they are rapidly destroyed by blood and brain enzymes and they are unable to cross the BBB.

The proposed project addresses these challenges by combining the potential of these peptides both as a targeting and effector molecules acting on the GPCRs on GBM cells while enhancing their stability and their brain permeability. To achieve this aim, lipidic groups will be anchored on peptides resulting in changes in their space orientation and formation of long strands with diameters of less than one thousandth of a millimetre known as nanofibers. We have shown that peptide nanofibers possess better stability in the blood and better permeation across the BBB. Utilising these GPCRs peptides, we can apart from delivering this anti-cancer peptides to the tumour, also use them as a carrier enveloping chemotherapeutic drugs within the core of these nanofibers potentiating further the therapeutic effects of the peptides by a synergistic anti-cancer effect and helping in shuttling and targeting conventional chemotherapeutic drugs to the main tumour mass, but also to the invading tumour cells.

This project, apart from answering critical questions regarding formation of peptide nanofibers from therapeutic peptides, is aimed at investigating how these nanofibers cross the BBB and how they activate the GPCRs and result in a potent anticancer response in human GBM cells. These studies will form the basis for the clinical translation of these peptides into a novel therapy for GBM sufferers. Although this project is aimed at targeting brain tumours, this nanotechnology-based approach can be used for the delivery of other therapeutic peptides for a wide range of brain tumours and neurological diseases and disorders and has profound potential implications within the field of clinical neurosciences.

## Endocrine therapies for Glioblastoma multiforme

**Glioblastoma; the unmet challenge.** Despite surgical debanking and improvements in radio- and chemotherapies, the prognosis of patients with GBM remains extremely poor. Particular challenges for GBM therapy include limitations in the extent of feasible surgical resections, distinct cellular heterogeneity, difficulties in drug delivery across the blood-brain barrier (BBB) and low drug distribution within the tumour. Although some cytotoxic drugs gain access to the major tumour mass by a virtue of damaged or incomplete blood-brain tumour barrier, such drugs fail to reach invading cancer cells surrounded by an intact BBB. Nanoparticulate technologies are the only technologies to-date to have shown promise in delivery across the BBB and in treatment of GBM.

**GnRH strong antitumour effect in GBM and limitations in its clinical translation**. The identification of the overexpression of Gonadotrophin Releasing Hormone (GnRH) G-protein coupled receptors (GPCRs) in biopsies from GBM sufferers and the strong antiproliferative,

antimetastatic, antiangiogenic dose dependent effects afforded by GnRH peptides linked to specific intracellular signalling cascades (Gai/cAMP pathway) makes them ideal novel therapies for gliomas if they could reach the tumour in adequate amounts. GnRH (pyroGlu-His-Trp-Ser$^4$-Tyr$^5$-Gly$^6$-Leu-Arg-Pro-Gly-NH2) possesses a short plasma half-life of 2-5 minutes mainly due to enzymatic plasma cleavage at the Glycine$^6$ residue. GnRH anchors to the GPCR transmembrane crevices mostly by hydrophobic interactions requiring both the N and C terminus of the decapeptide for binding while the N-terminus is critical for receptor activation. Several stable superagonists have been produced by modifying the Glycine$^6$ with a bulky apolar side-chain amino acids (e.g. triptorelin (D-Trp$^6$)). However, GnRH analogues are unable to cross the BBB in significant amounts due to their high molecular weight (>500 Da), propensity to hydrogen bond and hydrophilicity. Thus, attempts to benefit from their therapeutic potential has not been achieved.

Unlocking the GnRH therapeutic potential in GBM requires:

1. The development of stable agonists with enhanced binding capability to GnRH GPCRs.

2. A strategy to enable their permeation across the BBB.

3. An understanding of the molecular expression of the GnRH receptor in GBM patients

Herein we report a targeted endocrine delivery system based on self-assembled fibers derived from a lipidised GnRH peptide (TPGnRH). Lipidisation of GnRH with a palmitic tail at the Tyr$^5$ amino acid moiety confers amphiphilicity to the peptide allowing it to adopt a poly(proline) type II helix stabilising the self-assembled nanofibers. Fibers can bind and elicit a potent intracellular anticancer effect in GBM cells overexpressing the GnRH receptor. Paclitaxel, a model high molecular weight small-molecule anticancer drug that is effective in GBM, but does not cross the blood-brain barrier in effective amounts, is entrapped within the core of the stable peptide nanofibers and is rendered able to cross the BBB (30-fold increase in permeability) and target GBM cells.

## Project Milestones

The project milestones are summarised below:

Month 4 – Completion of molecular modelling studies resulting in identification of optimal lipidised analogue.

Month 6 – Synthesis and purification of 0.1 mmole scale for all lipidised analogues

Month 9 – Synthesis and purification of 1 mmole scale for all lipidised analogues

Month 10 – Characterisation of peptide nanofibers

Month 15 – Characterisation of drug loaded peptide nanofibers

Month 18 – Antiproliferative effects of peptide nanofibers assessed in immortalised human cell lines (U87MG)

Month 21 – Antiproliferative effects of peptide nanofibers assessed in low passage cell lines and assessment of expression of GnRH receptor in these cell lines

Month 24 – Permeability studies of nanofibers across an in vitro 3D all human BBB model; Data analysed, manuscripts prepared for publication, grant application for preclinical work submitted.

| | | Engineering novel endocrine nanomedicines for GBM | | | | | | | | | | | | | | | | | | | | | | | |
|---|---|---|---|---|---|---|---|---|---|---|---|---|---|---|---|---|---|---|---|---|---|---|---|---|---|
| | | Year ONE | | | | | | | | | | | | Year TWO | | | | | | | | | | | |
| | Measurable Outcomes\Months | 1 | 2 | 3 | 4 | 5 | 6 | 7 | 8 | 9 | 10 | 11 | 12 | 13 | 14 | 15 | 16 | 17 | 18 | 19 | 20 | 21 | 22 | 23 | 24 |
| MO1 | 1: Molecular modelling studies (Prof Tim Clark - Dr Lalatsa) | | | | | | | | | | | | | | | | | | | | | | | | |
| MO1 | 2:Synthesis of lipidised peptides (Dr Lalatsa) | | | | | | | | | | | | | | | | | | | | | | | | |
| MO1 | 3:Characterisation of peptide nanofibers and coated peptide nanofibers (Dr Lalatsa) | | | | | | | | | | | | | | | | | | | | | | | | |
| MO2 | Antiproliferative effects of peptide nanofibers (Dr Lalatsa- Prof Pilkington) | | | | | | | | | | | | | | | | | | | | | | | | |
| MO3 | GnRH receptor expression in low passage GBM cell lines (Dr Lalatsa- Prof Pilkington) | | | | | | | | | | | | | | | | | | | | | | | | |
| MO4 | Permeability studies across an in vitro 3D all human BBB mode (Dr Lalatsa- Prof Pilkington) | | | | | | | | | | | | | | | | | | | | | | | | |
| | Analysis and writing up | | | | | | | | | | | | | | | | | | | | | | | | |

**Milestone 1 (MO1) – 1; Molecular Modelling studies (Dr Lalatsa, Dr David Whittley)**

**Atomistic Simulations**; The structures of lipidized gonadotrophin releasing hormone amphiphiles were constructed in Molecular Operating Environment (MOE, Chemical Computing Group, Montreal, Canada) software. To construct a coarse-grained (CG) model of the tyrosyl-palmitoyl gonadotrophin releasing hormone (TPGnRH) amphiphile and validate the obtained angle distributions, atomistic simulations were carried out using the CHARMM36 forcefield in Gromacs 5.1.2. As CHARMM36 forcefield does not contain parameters for the region linking tyrosine to the palmitic tail, the initial parameters for this region were obtained from the CHARMM General Forcefield (CGenFF) server and further refined using Force Field Toolkit in Visual Molecular Dynamics (VMD). Due to lack of these parameters for aromatic lipidized peptides, modelling for these amphiphiles was not undertaken combined with the inability to synthesise stable O-lipidised aromatic tyrosyl analogues of GnRH using solid-phase peptide synthesis in high yield and able to assemble in nanostructures.

A single molecule of TPGnRH was immersed in a cubic box of TIP3P water, and a 50 ns MD simulation was carried out using Gromacs 5.1.2. All MD simulations were performed with periodic boundary conditions in all directions. All bonds were constrained using the LINCS algorithm and the time-step for integration was 2 fs. Temperature was maintained at 300 K using the Nosé-Hover thermostat and pressure was maintained at 1 bar using the Parrinello-Rahman scheme. The long-range electrostatic interactions were controlled using a particle-mesh Ewald approach with a real-space cut off of 1.0 nm and the Lennard-Jones interactions were cut off at 1.0 nm. All production simulations were done on the on the University of Portsmouth's Sciama High Performance Compute cluster.

**Coase Grained (CG) Model**; After parameterisation of the novel ester bond present on the GnRH peptide, a CG model of the TPGnRH was built based on the MARTINI forcefield. The basic principle of CG model is the simplification of the structure by grouping a cluster of atoms into a single particle or bead, thus reducing the overall number of particles in the system and when employed in MD allowing an increase in the value of the time step and the overall length of the simulation. Among the structure-based CG models, which use the native structural information of the target molecules as input, the MARTINI forcefield has been routinely used for in silico modelling of peptide amphiphiles. The MARTINI forcefield is centred on a four-to-one mapping, i.e. on average four heavy atoms including associated hydrogens are represented by a single interaction centre, a CG bead. Mapping of water is consistent with this four-to-one mapping, as four water molecules are mapped to a CG water bead. Small ring-like fragments or molecules (e.g., aromatic amino acid side-chains) are mapped with higher resolution of up two heavy atoms per one CG bead. To reproduce the chemical nature of the

system four main types of CG beads are defined: polar (P), nonpolar (N), apolar (C), and charged (Q). These four main types of beads are divided into subtypes distinguished either by a letter signifying hydrogen-bonding capabilities [donor (d), acceptor (a), both (da), and none (o)] or by a number representing the degree of polarity [ranging from 1 (low polarity) to 5 (high polarity)] giving a total of 18 bead particle types. The MARTINI mapping scheme provides a relatively straightforward and effective way of switching from the all-atom to a CG description of the molecule.

Following the CG methodology, the molecule was divided into 31 CG beads as shown in Figure 1. Interactions between the particles were treated with the Lennard-Jones interactions. The water model provided by MARTINI forcefield was used, in which one bead represents four molecules of water. For the region linking the Glu-GnRH to the palmitic tail, the mapping consists of a polar bead (18) representing the esteric oxygen and the carbonyl and four beads representing the Tyr residue of which 3 are apolar (15, 16, 17). As MARTINI forcefield is not capable of predicting changes in secondary structure, a β-turn type II was assumed for this peptide amphiphile based on the structure of the parent GnRH peptide. The resulting CG model was optimised, so that the distributions of the angles in the region linking $Tyr^5$ to the palmitic moiety obtained from CG simulations matched the distributions obtained with the atomistic simulation. The trajectory obtained from atomistic MD simulation was converted into a CG counter-part, the fine-grained (FG) trajectory, and the angle distributions for the CG and FG trajectories were calculated and compared using Gromacs 5.1.2. The following backbone angles were altered: the Tyr-Tyr-Pal (15-17-18) was increased from 127º to 150º, and the force constraint was increased from 20 to 25; Tyr-Tyr-Pal (16-17-18) was decreased from 127º to 100º and the force was increased from 20 to 25; Tyr-Pal-Pal (17-18-19) was reduced to 140º from the initial 180º; and Pal-Pal-Pal (18-19-20) was reduced from 180º to 140º. The two side-chain angles Tyr-Tyr-Tyr (14-15-16) and Tyr-Tyr-Tyr (14-15-17) were decreased from 150º to 110º and 140º, respectively. By altering the angles and force constraint, the distribution of the angles in the linking region in the CG model matched the atomistic simulation validating the CG model.

TPGnRH molecules were randomly inserted in the simulation box with random positions and orientations, and then the system was equilibrated and solvated with the appropriate number of CG water beads. MD simulations were carried out for 4.8 μs using a time step of 30 fs. The temperature of the system was maintained at 300 K using the Nosé-Hoover thermostat and the pressure was maintained at 1 bar using Parrinello-Rahman barostat. The coordinates were collected every 10,000 steps for analysis, and the trajectories obtained were visualised in VMD [295]. Simulations were repeated three times to investigate the stability of the obtained results.

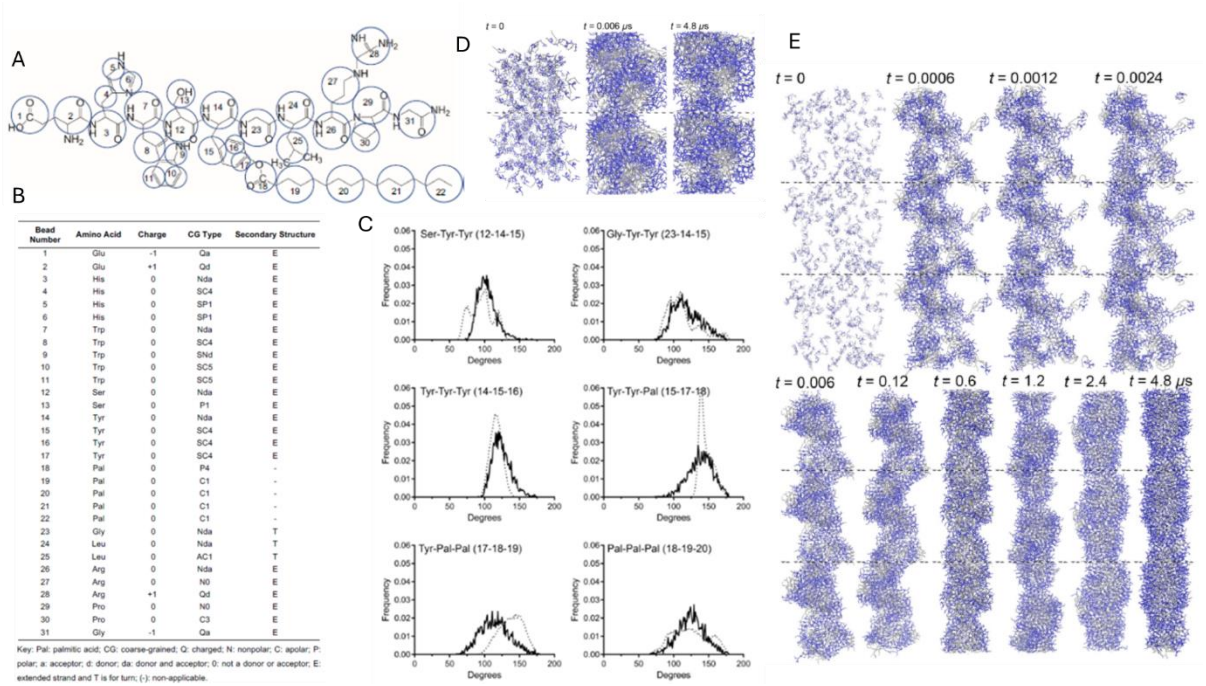


| Bead Number | Amino Acid | Charge | CG Type | Secondary Structure |
|---|---|---|---|---|
| 1 | Glu | -1 | Qa | E |
| 2 | Glu | +1 | Qd | E |
| 3 | His | 0 | Nda | E |
| 4 | His | 0 | SC4 | E |
| 5 | His | 0 | SP1 | E |
| 6 | His | 0 | SP1 | E |
| 7 | Trp | 0 | Nda | E |
| 8 | Trp | 0 | SC4 | E |
| 9 | Trp | 0 | SNd | E |
| 10 | Trp | 0 | SC5 | E |
| 11 | Trp | 0 | SC5 | E |
| 12 | Ser | 0 | Nda | E |
| 13 | Ser | 0 | P1 | E |
| 14 | Tyr | 0 | Nda | E |
| 15 | Tyr | 0 | SC4 | E |
| 16 | Tyr | 0 | SC4 | E |
| 17 | Tyr | 0 | SC4 | E |
| 18 | Pal | 0 | P4 | - |
| 19 | Pal | 0 | C1 | - |
| 20 | Pal | 0 | C1 | - |
| 21 | Pal | 0 | C1 | - |
| 22 | Pal | 0 | C1 | - |
| 23 | Gly | 0 | Nda | T |
| 24 | Leu | 0 | Nda | T |
| 25 | Leu | 0 | AC1 | T |
| 26 | Arg | 0 | Nda | E |
| 27 | Arg | 0 | N0 | E |
| 28 | Arg | +1 | Qd | E |
| 29 | Pro | 0 | N0 | E |
| 30 | Pro | 0 | C3 | E |
| 31 | Gly | -1 | Qa | E |

Key: Pal: palmitic acid; CG: coarse-grained; Q: charged; N: nonpolar; C: apolar; P: polar; a: acceptor; d: donor; da: donor and acceptor; 0: not a donor or acceptor; E: extended strand and T is for turn; (-): non-applicable.

Figure 1. **A**: CG mapping of TPGnRH based on the MARTINI forcefield and **B**: summary table of sequence, charge, bead type and secondary structure of TPGnRH amphiphile used in the CG simulations. **C**: Angle distributions from atomistic (dashed) and coarse grain (solid) models for the region linking Tyr5 and the palmitoyl moiety in TPGnRH [ $Ser^4$-$Tyr^5$ - O-Palmitoyl)-$Gly^6$]. The bead numbers of the amino acid residues are shown in parenthesis next to the bead sequence in B. **D**: Snapshot of the formation of TPGnRH aggregates. Simulation carried out with 128 molecules of TPGnRH and 6400 molecules of water (1:50) ratio in a cubic box of 20 nm for 4.8 μs. Hydrophobix tails are shown in grey and the peptide backbone in blue. Beads of water not shown for clarity. Black dotted lines represent periodic boundaries. **E**: **Snapshot of the formation of TPGnRH nanofibers in aqueous environment under periodic conditions**. Simulation carried out with 128 molecules of TPGnRH and 9600 molecules of water (1:75) ratio in a cubic box of 20 nm for 4.8 μs. Hydrophobix tails are shown in grey and the peptide backbone in blue. Beads of water not shown for clarity. Black dotted lines represent periodic boundaries.

A coarse-grained model was developed to overcome the time and length scale limitations of the classical atom-level molecular modelling. TPGnRH was built in the MOE software, and to later construct a CG model and validate the obtained angle distributions, atomistic simulations were carried out using the CHARMM36 forcefield. Then, a CG model of TPGnRH was built based on the MARTINI forcefield using a four-to-one mapping (Figure 1). Based on a previous work with a palmitoylated peptide amphiphile [1], the phenolic ester linking the $Tyr^5$ to the palmitoyl moiety consisted of a polar bead including the hydroxyl and the carbonyl group (bead 18), and three beads representing the $Tyr^5$ residue (beads 15, 16, 17). The CG model consisted of 31 interaction sites, which significantly reduces the number of particles in a system allowing an increase in the value of time in MD simulations. To validate this CG model of the phenolic ester, the angle distributions from a fine-grained (derived from the atomistic model) trajectory were compared to the angle distributions of the CG model (Figure 1C).

The angle distributions of the CG model match well the angle distributions that were derived from the atomistic model confirming the validity of the model to further MD simulations. The obtained angle distributions of the beads representing the $Tyr^5$ and the palmitic tail (14-15-16, 15-17-18, 17-18-19, 18-19-20) are similar to the ones reported for palmitoylated dalargin [1]. Atomistic model of the palmitoylated dalargin showed angle distributions ranging from 100-150, 125-150, 100-175 and 75-175º for Tyr-Tyr-Tyr (14-15-16), Tyr-Tyr-Pal (15-17-18), Tyr-

Pal-Pal (17-18-19) and Pal-Pal-Pal (18-19-20) respectively, which are in accordance with our results (Figure 1C). The CG model of the palmitoylated dalargin was refined by reducing the angle of the Pal-Pal-Pal (18-19-20) bead from 180 to 140º. In the TPGnRH model, the same angle was altered from 180 to 140º, however, to achieve a better matching of the CG with the atomistic model, other angles were also altered in our CG model. These alterations provided a superior level of similarity between the atomistic and the CG, which give us more confidence in the developed CG model.

Using the CG model, MD simulations were conducted with 128 molecules of TPGnRH in a range of peptide to water molar ratios (1:10, 1:25, 1:50, 1:75, and 1:100). At the lower water ratios, such as at 1:10, 1:25, and 1:50, TPGnRH self-assembled into large nearly spherical aggregates that are associated with the aggregates in the neighbouring boxes. This organisation occurs from the onset of the simulation (> 0.006 μs) and remains unaltered as time progresses until the end of the simulation at 4.8 μs (Figure 2.20). Thus, at low hydrophobic strength and insufficient water CG beads in the box, the position of the palmitic tails lacks a coherent orientation forming open structures with hydrophobic and hydrophilic regions.

When the peptide to water ratio was increased to 1:75 and 1:100, spontaneous self-assembly of TPGnRH into a nanofiber was observed (Figure 1). During the early steps (0-0.0024 μs), peptide self-assembled into aggregates as seen with the lower peptide to water ratios. The hydrophobic palmitic tails orientate forming hydrophobic aggregates while the peptide backbone is exposed to the surface along with polar amino acids (Glu1, Arg8 and Gly10-NH2). Between the 0.006-0.12 μs time interval, as the hydrophobic interaction strength increased, the amphiphile starts forming a long-axial nanostructure with a high curvature and with hydrophobic cores formed by the palmitic tails. At 0.6 μs, the peptide amphiphile started rearranging into a single nanofiber with a low curvature and an organised hydrophobic core. A similar behaviour was described for other amphiphile, in which the self-assembly started with the formation of the roughly spherical/open aggregates (0.1-1 μs) followed by the rearrangement into a single nanofiber at 16 μs [2]. Simulations of the TPGnRH at 4.8 μs exhibited ribbon-like peptide nanofibers consisting of repeating grooves with a diameter of 50.86 Å and 41.81 Å at middle and end of groove, respectively. Each groove has a length of 105.51 Å. Due to the periodic conditions, the length of the fibers cannot be determined and is considered infinite. The hydrophobic palmitic tails collapse in the hydrophilic environment towards the core of the nanofiber while the peptide backbone and the polar amino acids are orientated towards the surface. The amino acids involved in binding to GnRH-R ($Glu^{1}$-$His^{2}$-$Trp^{3}$ and $Arg^{8}$-$Pro^{8}$-$Gly^{10}$-NH2) [3] are positioned at the surface (Figure 2), and this is of particular importance to ensure that the peptide amphiphile maintains its biological activity.

Thus, modelling studies support the self-assembly of O-palmitoylated lipidized GnRH amphiphiles maintaining critical amino acids for binding available towards the surface of the nanofibers and able to interact with GnRH receptor (GnRHR).

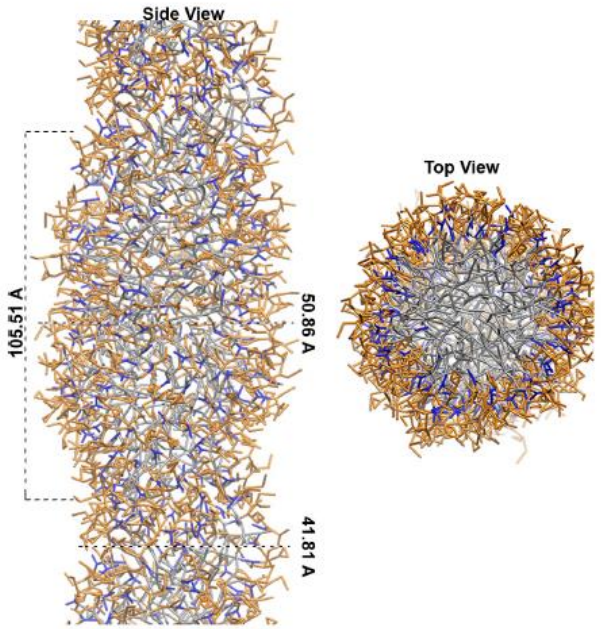


Figure 2. Snapshot of the side and top views of a TPGnRH nanofiber formed in silico. Beads for the amino acids involved in binding and activation of the GnRH receptor (GNRHR) are coloured in orange (Glu-His-Trp and Arg-Pro-Gly-$NH_2$), while the remaining amino acids are in blue. Hydrophobic tails are represented in grey.

Figure 2. Snapshot of the side and top views of a TPGnRH nanofiber formed in silico. Beads for the amino acids involved in binding and activation of the GnRH receptor (GNRHR) are coloured in orange (Glu-His-Trp and Arg-Pro-Gly-NH2), while the remaining amino acids are in blue. Hydrophobic tails are represented in grey.

**Milestone 1 (MO1) – 2 and 3; Synthesis of lipidized peptides and characterisation (Dr Lalatsa)**

Manual synthesis of Glu-GnRH and of the lipidised Tyr5 (O-Palmitoyl)-GnRH, TPGnRH, was carried out using an orthogonal solid phase peptide synthesis (SPPS) protocol at a scale between 0.1 to 0.5 mmol in glass peptide synthesis reaction vessels with a 0.1 µm frit and the diameter varying between 3-5 cm (Figure 3A). Peptides were synthesised in a rink amide MBHA resin (200 µm of mesh, 0.59 mmol $g^{-1}$), pre-swelled in DMF for one hour under continuous stirring (Mains Stuart Flask Shaker, Bibby Scientific Ltd, Staffordshire, UK). Fmoc-protected amino acids (4.2 eq.) were activated with HBTU (4.0 eq.) and DIPEA (5.0 eq.) and coupled twice for 45 minutes each time under shaking. The orthogonal strategy involved the use of the following side-chain protecting groups: Glu (tBu), His (Trt), Trp (Boc), Ser (tBu), Tyr(2-ClTrt) and Arg (Pbf). To activate the N-a-protected amino acid for the coupling to the linker, HBTU was added to the first amino acid, and then transferred to the reaction vessel. Addition of DIPEA followed to ensure proper kinetics of coupling. After coupling each residue, Kaiser test was performed to confirm a complete coupling prior the deprotection and addition of the next amino acid. Removal of the Fmoc moiety was achieved by adding piperidine [20% (v/v) in DMF, ~ 10 mL] to the resin and agitating the reaction vessel for 10 minutes. All peptide synthesis was carried out at room temperature. Once the peptide sequence was complete, Fmoc deprotection was achieved using 20% (v/v) piperidine solution in DMF, and the resin beads were washed with DMF followed by a mixture of DCM:MeOH (1:1). Resin beads were dried under vacuum and transferred into a pre-weighed glass vial. The beads were stored in a silica desiccator overnight before the cleavage of the peptide from the resin.

Cleavage of the peptides from the resin was achieved using 1 mL of cleavage mixture [TFA:TIS:H2O (95:2.5:2.5)] for each gram of dry resin for 4 hours, at room temperature, under stirring. The cleavage mixture was filtered using filter paper and the filtrate was then collected

in a round bottom flask. TFA was rotaevaporated under vacuum during 4 hours using a liquid nitrogen trap. After rota-evaporation, the crude peptides were precipitated using cold diethyl ether at (-20 °C). The precipitated peptides were collected using centrifugation (1,200 rpm for 15 minutes, Jouan B4i centrifuge, Thermo Scientific, Paisley, UK). The supernatant was discarded and the peptide was resuspended in cold diethyl ether. The washing and centrifugation steps were performed twice, and the peptides were re-suspended in de-ionised water and freeze-dried over 48 hours in Edwards Modulyo® Freeze Dryer (Thermo Scientific, Paisley, UK) attached to a vacuum pump system 320015 (Gardner Denver Ltd., Medstead, UK).

The esterification of the free phenolic hydroxyl group of $Tyr^5$ of Glu-GnRH was achieved by attaching a palmitic tail as previously described. The Tyr- Gly-Leu-Arg-Pro-Gly was synthesised as above. The 2-chlorotrityl protecting group of the side chain of the tyrosyl residue was removed by reacting the DCM:MeOH (1:1) dried beads with the freshly prepared cleavage solution [DCM:TFA:TIS (90:5:5)] for 10 minutes, under constant stirring. The latter step was repeated four times in total. Beads were washed with DCM:MeOH, and then DMF prior to allowing them to swell for at least one hour in DMF under shaking. For esterification of the phenolic –OH of Tyr5, N-hydroxysuccinimide ester of palmitic acid (8.0 eq.) in ~ 4 mL of DMF and triethylamine (16.1 eq.) were added to the beads in DMF, and the reaction was left to proceed for 24hours under constant stirring at room temperature. Once the reaction was completed, beads were washed with copious amounts of DMF and remaining synthesis was continued as described above. Crude peptides were purified using solid phase extraction (Sep-Pak plus C18 column, Waters).

The yield of the crude Glu-GnRH and TPGnRH were calculated to be 68% and 32% (25-48%) respectively with purity >90% resulting in a retention time of 21.34 minutes. After purification using solid phase extraction, a purity between 95-99% was observed for fractions eluted at 45-60% acetonitrile and water mixtures for TPGnRH and fractions eluted with 15-45 % acetonitrile water mixtures. Purified fractions were pooled together and used for further characterisation or testing.

Esterification of the phenolic hydroxyl group of $Tyr^5$ was supported by reverse phase HPLC (Figure 3B), mass-spectrometry (Figure 3C), NMR (Figure 3E), Fourier-transformed infra-red spectra (Figure 3 D). Assignment of the peak on NMR was feasible using 1H-1H TOCSY spectra provided information of protons that are connected through a bond (usually, no more than 3 bonds apart) and 1H-1H NOESY confirmed the proximity of the palmitic tail to core of the fiber similar to in silico studies. Mass spectrometry exhibited the m/z of 1437.56 Da in agreement with the calculated mass (1438.73 Da).

Pyrene assay demonstrated the ability of the TPGnRH to self-assemble into aggregates at critical aggregate concentrations (CAC) of 7 µM (Figure 4c), while thioflavin T suggested that at a minimal CAC of 135 µM, TPGnRH forms long-axial nanofibers (Figure 4d). TPGnRH (70-700 µM) was visualised by TEM (Figure 4i) and AFM (Figure 4j). At low concentration, TPGnRH formed quasi-spherical aggregates with 985.55 ± 0.19 (n=10) of diameter, as calculated by TEM imaging analyses. With the increase of TPGnRH concentration, above the CAC calculated using the thioflavin T assay, the amphiphile self-assembled into ribbon-like nanofibers with the diameter of 17.06 ± 5.31 nm (n=10) obtained by TEM, and 5.72 ± 3.93 to 19.84 ± 0.22 nm (n=10) determined by AFM. At low concentrations (70 µM), TPGnRH assumed a β-turn type II as described for the parent peptide involving $Tyr^5$-$Gly^6$-$Leu^7$-$Arg^8$, however when in the nanofiber conformation, TPGnRH adopted the conformation of a polyproline type II (PPII) helix (Figure 4e and 4k). CD spectra of the fibers exhibited a maximum at 228 nm and a strong negative peak at 205 nm, which are the hallmarks of a PPII,

and an isodichroic point at 205 nm over a range of temperature confirming the PPII 11 (Figure 4g). The collapse of the palmitic tails into a hydrophobic core forces the peptide backbone to be exposed at the surface allowing it to interact by hydrogen bonding with the water molecules of aqueous media and stabilise into a PPII helix. Most importantly, CD studies at the range of temperatures (15-50 °C) and dilutions (1:10-1:100) show the physical stability of the nanofibers (Figure 4f,h) in comparison to the micelles.

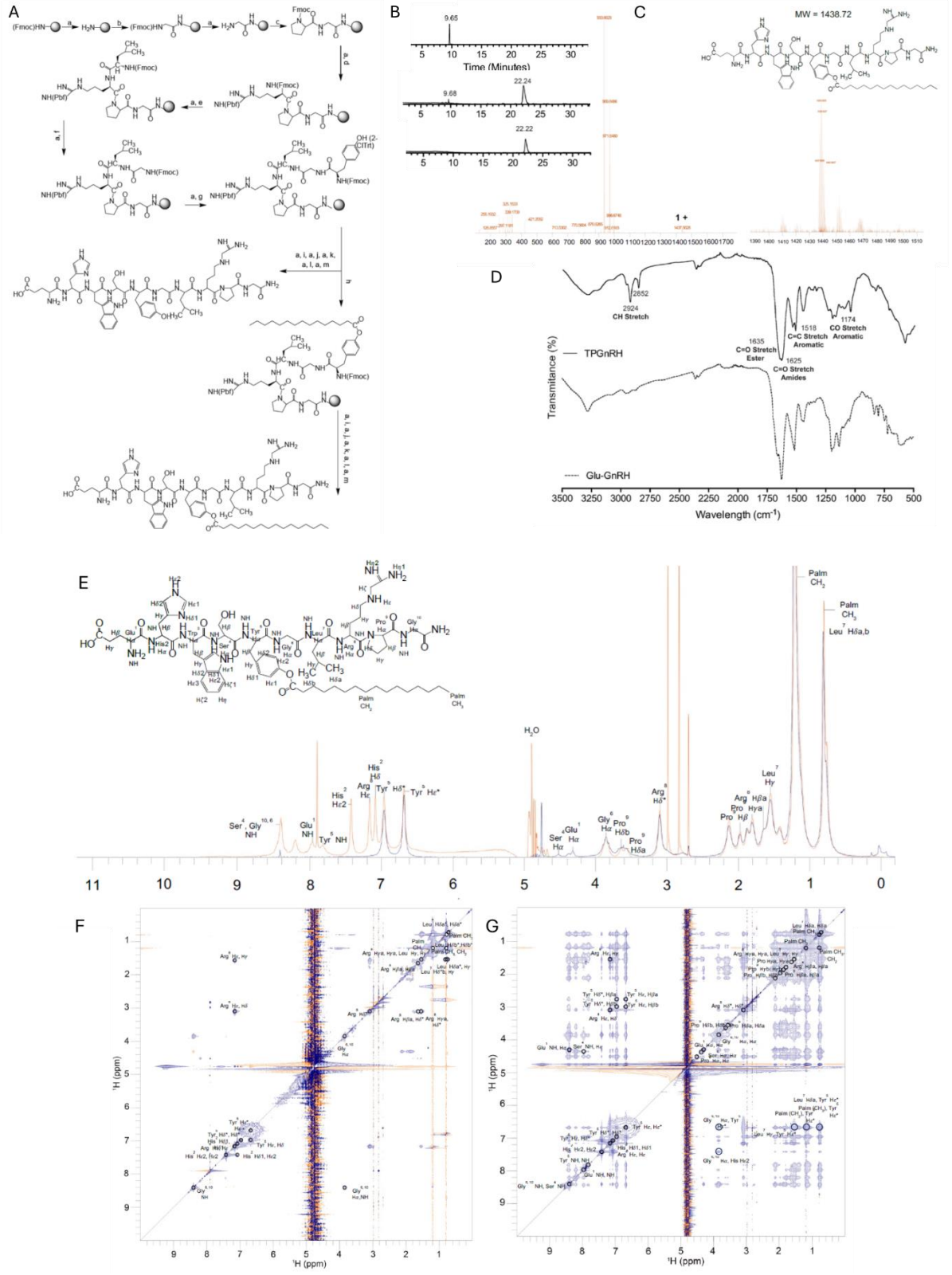

Figure 3. **A**: **Schematic of the solid phase peptide synthesis of TPGnRH analogues**. a) piperidine 20% (v/v) in DMF for 10 minutes, twice, b) Fmoc-Gly-OH, c) Fmoc-Pro-OH, d) Fmoc-Arg(Pbf)-OH, e) Fmoc-Leu-OH, f) Fmoc-Gly-OH, g) Fmoc-Tyr(2-ClTrt)-OH, HBTU and DIPEA in DMF for 45 minutes twice, h) TFA:TIS:DCM (5:5:90) for 4 times, 10 minutes, palmitic acid N-hydroxysuccinimide ester (8 eq.) and triethylamine (16.1 eq.) in DMF and i) Fmoc-Ser(tBu)-OH, j) Fmoc-Trp(Boc)-OH, k) Fmoc-His(Trt)-OH, and l) Fmoc-Glu(OtBu)-OH, HBTU and DIPEA in DMF, m) TFA:TIS:$H_2O$ (95:2.5:2.5) for 4 hours, rotary evaporation and precipitation in cold diethyl ether. The Fmoc-amino acids (4.2 eq.) were activated with 4.0 eq. HBTU and 5.0 eq. DIPEA. **B**: Example of **RP-HPLC chromatograms** of crude Glu-GnRH (top), crude TPGnRH (middle) and solid-phase extraction purified TPGnRH (bottom). The Glu-GnRH and TPGnRH peptides were dissolved at 200 µg $mL^{-1}$ in a mixture of acetonitrile and water (50:50) and absorbance was recorded at 220 nm. Purity of the crude Glu-GnRH was 97.4% showing a peak at 9.65 minutes. The crude and purified TPGnRH exhibited a purity of 93.45% and > 99.0%, respectively, with a retention time at 22 minutes. **C**: **Electrospray ionisation MS spectrum** TPGnRH. Peptide sample (1 mg) was dissolved in 1 mL of a mixture of acetonitrile and 0.1% (v/v) formic acid (52.5:47.5) and infused at a rate of 5 µL $min^{-1}$. Spectrum in the right side shows the region from 1390-1500 mass/charge ratio in detail of TPGnRH. Calibration (Cal.) using CsI (cesium iodide) (m/z = 132.9) and a peptide (m/z = 829.5). **D**: **Fourier transformed infrared (FTIR) spectra** of Glu-GnRH and TPGnRH. **E: $^1$H-NMR spectra of TPGnRH** at 600 MHz. Purified TPGnRH (> 95% purity, determined by HPLC) was dissolved in a mixture of $H_2O$ and $D_2O$ (90:10) (orange) or $D_2O$ (blue) at concentration of 15 mM (pH 4.5). Key: Palm: palmitoyl; *: indicates the signal of 2 protons. **F: 1H-1H TOCSY spectra of TPGnRH**. Purified TPGnRH (> 95% purity determined by HPLC) was dissolved in a mixture of 90% H2O and 10% $D^2O$ at a final concentration of 15 mM (pH 4.5). Key: Palm: palmitoyl; *: indicates the signal of 2 (or 3 protons in Leu Hδ). **G: 1H-1H NOESY spectra of TPGnRH**. Purified TPGnRH (> 95% purity determined by HPLC) was dissolved in 90% $H_2O$ and $D_2O$ to 15 mM at pH 4.5). Key: Palm: palmitoyl; *: indicates the signal of 2 protons or (3 in Leu Hδ).

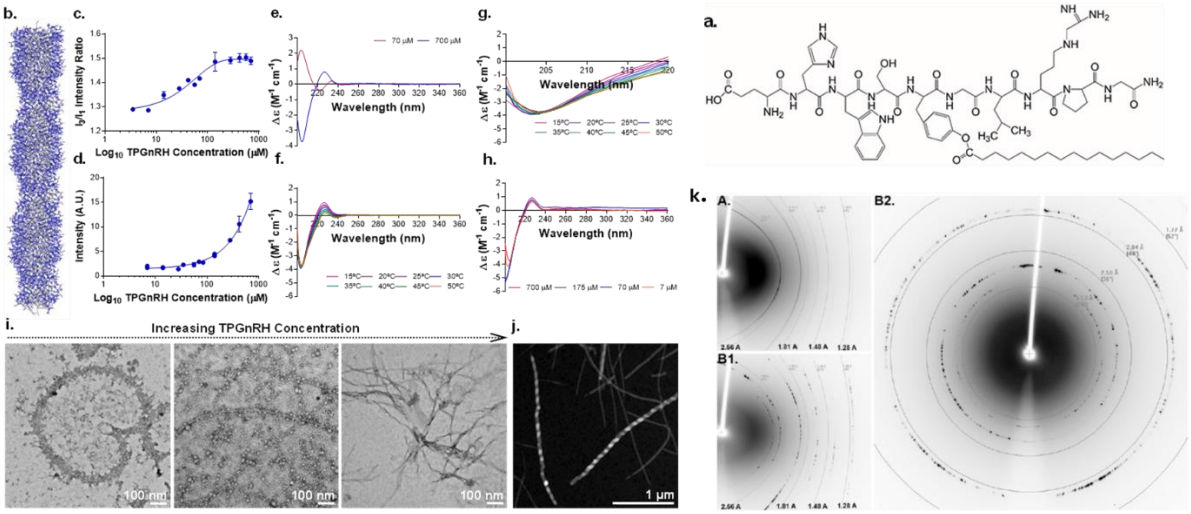


Figure 4. Conformation of TPGnRH nanofibers in an aqueous environment. (a) Chemical structure of the lipidised GnRH, TPGnRH. (b) Coarse-grained molecular dynamics simulation of the peptide nanofibers (128 molecules of peptide in 9600 molecules of water in a cubic box of 20 nm for 4.8 µs). Hydrophobic tails are presented in grey and peptide backbone in blue. Beads of water are not shown for clarity. (c) Pyrene and (d) thioflavin T fluorescence assays to obtain the critical concentration aggregation (CAC) for vesicles and nanofibers respectively. Mean ± SD (n=3). (e) Circular dichroism (CD) spectra of TPGnRH at 70 (pink) and 700 µM (blue). (f) CD spectra of TPGnRH at a range of temperatures (15-50 °C). (g) CD spectra of TPGnRH at 700 µM a range of temperatures showing the isodichroic point at 205 nm. (h) CD spectra of TPGnRH at a range of dilutions. (i) Transmission electron microscopy (TEM) of the TPGnRH at increasing concentrations (70, 420 and 700 µM) in PBS (0.01 M, pH 7.4). Staining using 2% (w/v) uranyl acetate. (j) Atomic force microscopy (AFM) of TPGnRH at 1400 µM. (k) Two-dimensional X-ray diffraction images of TPGnRH. TPGnRH (A) vesicles (70 µM) and (B1, B2) nanofibers (700 µM) patterns measured from dried stalks.

The hydrophobic core formed by the palmitic tails in the TPGnRH nanofibers was used to entrap a brain impermeable drug, paclitaxel (PTX). The encapsulation of PTX was achieved using a solvent evaporation method with a constant amount of PTX (3 µmol, 2.562 mg) and increasing amounts of TPGnRH to obtain a range of PTX to TPGnRH molar ratios (1:1, 1:2, 1:3.7, 1:7.4). Encapsulation efficiencies increased with the amount of amphiphile reaching 68.67 ± 3.59% at the PTX:TPGnRH molar ratio of 1:7.4 (Fig. 5a). At this ratio, the aqueous solubility of PTX is 1759.21 ± 91.98 µg $mL^{-1}$, which is ~ 1900-fold higher than the aqueous solubility of PTX in an aqueous buffer solution (0.92 ± 1.35 µg $mL^{-1}$). The formulation of PTX:TPGnRH (1:7.4 mol/mol) affords the solubilisation of clinically relevant amounts of PTX as the formulation of PTX (Taxol®) allows a final concentration of 300-1200 µg $mL^{-1}$ in a mixture of Cremophor and ethanol (50:50). The PAX-loaded TPGnRH formulation was characterised in terms of morphology (Fig. 5b, c). TEM images showed the presence of thin and short nanofibers with a diameter of 9.48 ± 2.54 nm (*n*=10) and an average length of 199.96 ± 46.05 nm (*n*=10) that are associated with vesicles of 5.16 ± 0.66 nm (*n*=10). The AFM images further confirmed the ribbon-like structure of the PTX-loaded nanofibers with a diameter of 3.74 ± 2.15 nm (*n*=10). PTX-loaded TPGnRH nanofibers showed no alterations in the diameter in comparison to the unloaded fibers (*p:*0.9876), however the groove size of the fibers significantly increased in the presence of PTX (84.0 ± 16.73 nm *versus* 47.67 ± 17.70 nm) suggesting the accommodation of PTX within the core of the nanofibers. Based on the interaction of PTX with the β-subunits of tubulin, we can suggest that the 3'-benzoamido phenyl, 3'-phenyl, and 2-benzoyl phenyl of the PTX interact by hydrophobic interactions with the palmitic tail and hydrophobic amino acids orientated towards the core of the nanofibers.

The release studies of PTX-loaded TPGnRH in 1% (w/v) Soluplus® in PBS exhibited a gradual release over the first 24 hours (< 60% PTX) followed by a plateau (Fig. 5d). Slow release of PTX from the nanofibers limits the free amount of drug in the circulation limiting the bone marrow toxicity of PTX. In addition to the physical stability of TPGnRH, the enzymatic stability of PTX-loaded nanofibers was studied in relevant biological media (Fig. 5e, f, g, h).

Similarly to unloaded fibers, PTX-loaded TPGnRH showed an enhanced stability in all homogenates compared to the parent peptide (Glu-GnRH). In the plasma and brain homogenates, the nanofibers exhibited a slow degradation with > 80% of the peptide remaining stable and following a zero-order degradation profile. In the liver homogenates, TPGnRH nanofibers follow a first-order two-phase exponential with a fast degradation within the first hour followed by a slow degradation with 50% of the remaining peptide. Glu-GnRH profiles followed a first-order exponential decay ($r^2$ > 0.99) with the breakdown of the peptide, mainly, by the endopeptidase 24.15 (EP 24.15) at the $Tyr^5$-$Gly^6$. The discrepancies in Glu-GnRH and TPGnRH profiles allow us to propose that the modification at a $Tyr^5$ in the lipidised analogue confers resistance to the enzyme EP24.15 and that the degradation is, conceivably, mediated by other enzymes (such as, esterases). Hence, the slow release of PTX from PTX-loaded nanofibers, stability in the plasma (and other relevant tissues) and the low haemolytic toxicity with an $IC_{50}$ of 200 µM are promising for the clinical translation of the nanomedicine.

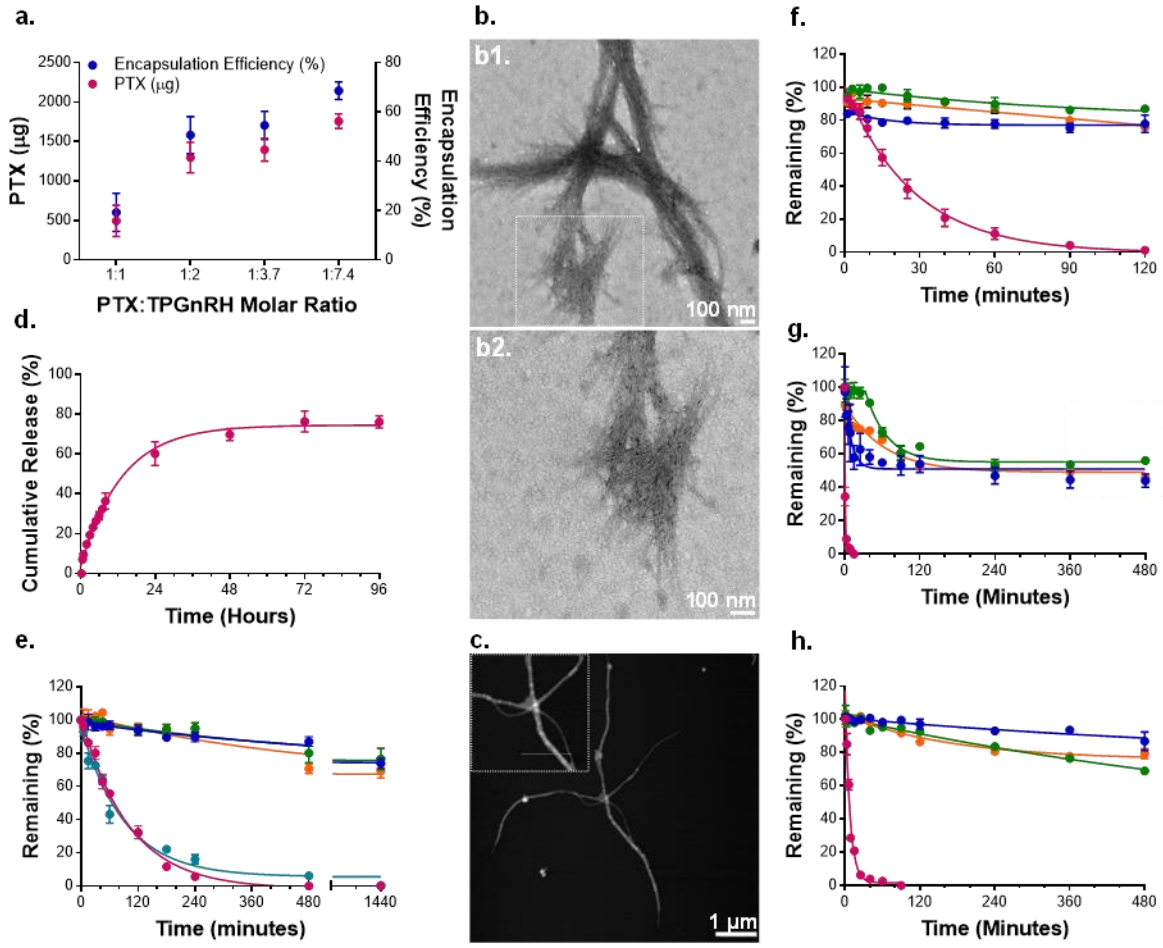


**Figure 5. Stable PTX-loaded TPGnRH nanofibers**. (a) Encapsulation studies with a varying amount of TPGnRH and equal amount of PTX (3 µmol). Mean ± SD (n=3, three independent studies). (b) TEM and (c) AFM image of PTX-loaded TPGnRH (1:7.4) nanofibers. Staining of the nanofibers using 2% (w/v) uranyl acetate. (d) Release of PTX from PTX-loaded nanofibers in 1% (w/v) Soluplus in PBS (0.01 M, pH 7.4). Mean ± SD (n=3). (e) Stability of PTX-loaded TPGnRH in homogenates from human GBM cells (U-87 MG) cells (protein concentration of 1 mg $mL^{-1}$). (f) Stability in 50% (v/v) rat plasma (protein concentration 8.76 ± 0.10 mg $mL^{-1}$), (g) 50% (w/v) rat liver homogenate (protein concentration 63.36 ± 4.79 mg mL-1), and in (h) 50% (v/v) rat brain homogenate (protein concentration 8.27 ± 0.43 mg mL-1) of the PTX-loaded nanofibers. Glu-GnRH: pink; goserelin: light blue; TPGnRH: dark blue; PTX-loaded TPGnRH: green; PTX: orange. Mean ± SD (n=3, two independent studies).

**Milestone 2 (MO2); Antiproliferative effects of peptide nanofibers assessed in immortalised human cell lines (U87MG) (Dr Lalatsa, Prof Pilkington, Prof Hinterdorfer (Linz, Austria))**

*Binding of Nanofibers to GnRH Receptors (GnRHR) overexpressed on GBM Cells*

The interaction of TPGnRH nanofibers with the GnRHR expressed on living U-87 MG glioma cells was studied using single force molecular spectroscopy (SMFS) and topography and recognition imaging (TREC). When attached to the AFM tip *via* a covalent bond, GnRH-R agonists demonstrated the ability to bind to the receptor expressed on U-87 MG cells, which is exemplified by the unbinding events on the force-distance curves. Glu-GnRH and TPGnRH nanofibers showed a binding probability of 13.3 ± 1.91 and 13.2 ± 0.9%, respectively, to GnRH-Rs on U-87 MG cells (Fig. 6a). Although the monomers of the TPGnRH and goserelin

(commercial stable GnRH analog) assume a favourable conformation (β-turn type II) for the binding to the GnRHR that was not reflected in a higher binding probability to the receptor on U-87 MG. The greater binding probability of the TPGnRH nanofibers is, possibly, explained based on their morphology. Unlike a small molecule that displays a single binding site, the TPGnRH nanofibers exhibit multiple binding sites on the surface ($Glu^{1}$-$His^{2}$, $Arg^{8}$-$Pro^{9}$-$Gly^{10}$) and their decreased curvature allows the display of those amino acids and the binding to the GnRH-Rs (multivalency). A similar binding force was obtained for all the GnRH analogues (Fig. 6b) suggesting that the binding occurs in the same binding pocket, possibly, involving the amino acids $Lys^{121}$, $Asn^{102}$ and $Asp^{302}$ of GnRHR and $Gly^{10}$-$NH_2$, $Arg^{8}$ and $His^{2}$ of the GnRH [22]. Using SMFS, the dissociation rate ($K_{off}$) was obtained for the distinct GnRH analogues (Fig. 6c). Interestingly, goserelin and TPGnRH have a lower $K_{off}$ than the Glu-GnRH, which is then associated to a longer residence time within the receptor binding pocket. The time of residence of TPGnRH nanofibers suggests that this GnRH analogue might have an improved *in vivo* efficacy, as the longer the receptor-ligand complex endures, the longer the effect of the drug.

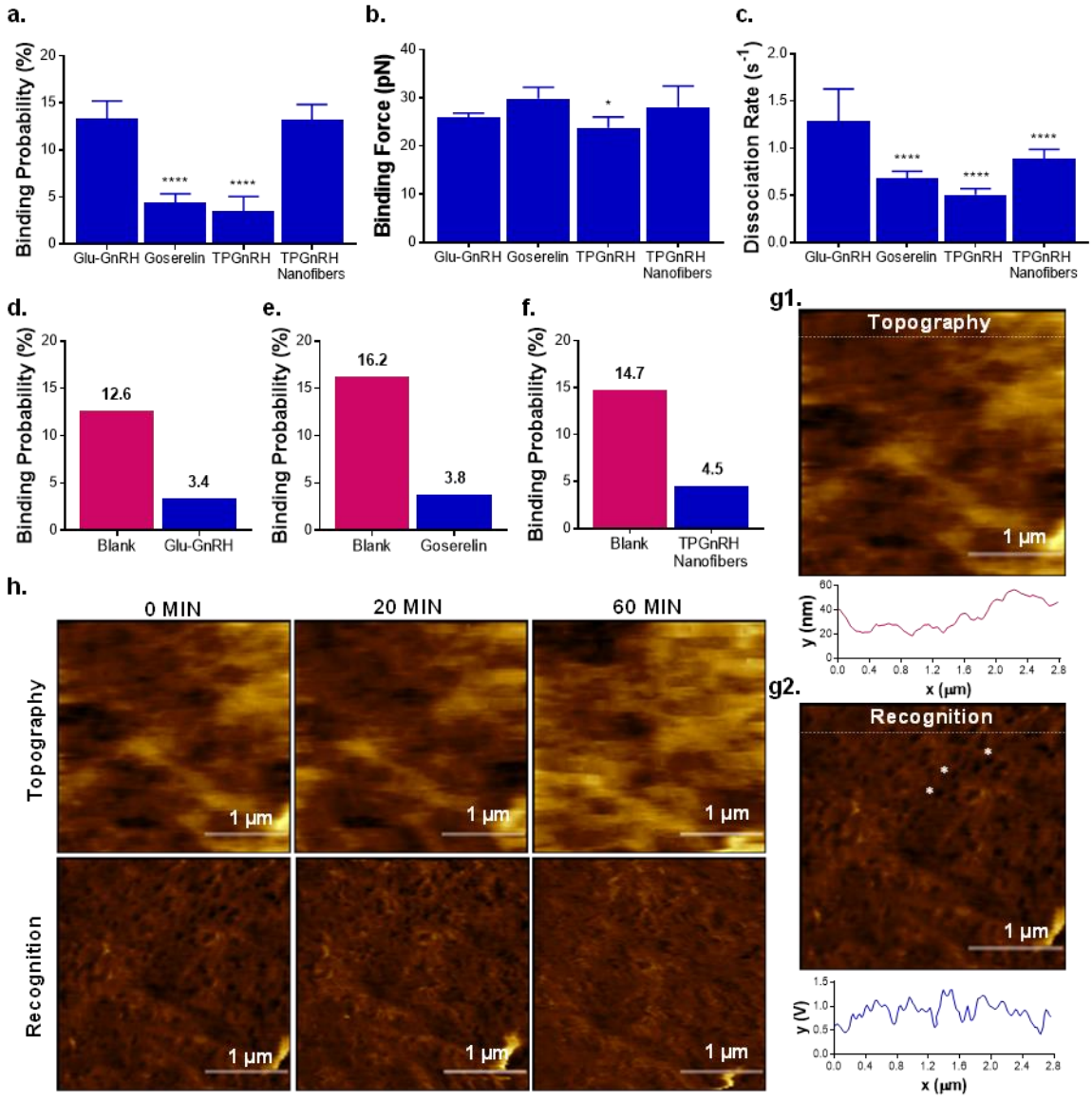


**Figure 4. Specificity of TPGnRH nanofibers to GnRHR GPCRs.** (a) Binding probability of the GnRHR ligands to the GnRHR on living GBM cells (U-87 MG). Retraction speed of the AFM tips at 1 µm $s^{-1}$. Mean ± SD (*n*=5 cells, > 1000 curves per cell). **** *P*<0.0001, comparing the GnRHR ligands to Glu-

GnRH (One-Way ANOVA with a Tukey's post-hoc). (b) Binding force of the GnRHR ligands to GnRHR binding pocket. Retraction speed of the tips 1 μm $s^{-1}$. Mean ± SD (*n*=5 cells, > 1000 curves per cell). * *P*<0.05, comparing GnRH-R ligands to Glu-GnRH (One-Way ANOVA with a Tukey's post-hoc). (c) Dissociation rates of the GnRH-R ligands on U-87 MG cells. Analysis at a retraction speed of 1 μm $s^{-1}$. Mean ± SD (*n*=6-14 cells, > 1000 curves per cell). **** *P*<0.0001, comparing the GnRH-R ligands to Glu-GnRH (One-Way ANOVA with Tukey's post-hoc). (d, e, f) Binding probability of TPGnRH nanofibers to GnRH-R on the GBM cells before (blank) and after the addition of a GnRH-R ligand (Glu-GnRH, goserelin, TPGnRH nanofibers). Retraction speed 1 μm $s^{-1}$. (g) TREC analysis of the cell surface of U-87 MG cells using AFM tips functionalised with TPGnRH nanofibers. (g1) Topographical image and a plot showing the differences in height of the cell along the $x$ (μm) direction. (g2) Recognition image of the same topographical area with some binding spots marked with an asterisk and a plot of the amplitude of the tip along the $x$ (μm) direction. Scale bar: 1 μm. Topography scale: 0-100 nm. Recognition scale: 0-4 V. (h) Specificity of the TPGnRH nanofibers to the GnRHR on U-87 MG cells. Topography and recognition images at time 0 (before addition of free TPGnRH) and after addition of the free nanofibers (20 and 60 minutes) able to bind to the receptors and limit the binding of TPGnRH-functionalised tips to the GnRHR.

Blocking experiments using GnRHR ligands were carried out to confirm the specificity of the TPGnRH nanofibers to the GnRH-R (Fig. 6d, e, f). After one hour of incubation of the U-87 MG cells with free ligands, the binding probability of the TPGnRH nanofibers attached to AFM tips was significantly reduced (a 2 to 4-fold decrease). Topographical image (Fig. 6g1) depicts the landscape of ~ 2 x 2 $\mu m^2$ of a U-87 MG cell showing a roughly smooth cell surface. The simultaneously recorded map for recognition displays the location of the binding events (dark spots) corresponding to the binding of the TPGnRH nanofibers attached to the AFM tip to the GnRH-R on the surface of the cells (Fig. 6g2). These recognition spots are irregularly distributed on the cell surface and reflected in nanodomains with variable dimensions ranging from ~ 10 to 90 nm (mean 48.0 ± 24.84 (*n*=20). Spots with dimensions of ~ 5-10 nm are attributed to single active GnRH-R considering the size of the GnRH-R (~ 3 nm and the free orientation of the PEG-linker (~ 6nm). Blocking experiments using TREC further confirmed the TPGnRH specificity for the GnRH-Rs (Fig. 6h). Addition of free nanofibers caused an alteration in the recognition maps with a disappearance of the binding spots corresponding to the binding of TPGnRH to GnRH-R on the cell surface along the time.

*Antitumour Effect of Nanofibers on GBM Cells (U-87 MG cells)*

*In vitro* antitumour effects of TPGnRH nanofibers were assessed on U-87 MG cells (a GnRH-$R^+$ cell line) and SK-OV-3 (GnRH-$R^-$ cell line). After 6 days of treatment, an $IC_{50}$ of 10.34 ± 3.46 μM was obtained for U-87 MG cells while in the SK-OV-3 the $IC_{50}$ value is > 100 μM (Supplementary Fig. 10) confirming the specific targeting of the nanofibers to GnRH-R. Cytotoxicity studies of PTX on U-87 MG showed a strong antitumour effect with an $IC_{50}$ of 2.82 nM after 6 days treatment. TPGnRH and PTX-loaded TPGnRH downstream effects on U-87 MG cells were further assessed in terms of cell metabolic activity, proliferation, cell cycle and apoptosis (Fig. 7). After the 6 days treatment, TPGnRH nanofibers significantly reduced (*P*<0.0001) cell metabolic activity to 49.16 ± 4.98% and 6.72 ± 1.37% when added at 7 and 35 μM. PTX-loaded nanofibers in combination with TPGnRH resulted in an additive effect (Fig. 7a) at low concentration of TPGnRH (7 μM). At high concentrations of TPGnRH (> 35 μM), PTX-TPGnRH nanofibers effects are masked by the low cell number after two doses of the nanofibers. To further understand the effect of TPGnRH, a BrdU and cell cycle assays were carried out (Fig. 7b, c). BrdU assay confirmed the antiproliferative effect of these nanofibers on U-87 MG at concentrations > 7 μM, and the cell assays clarified that the effect on proliferation is due, at least in part, to cell cycle arrest at the G2/M phase of the cell cycle of GBM cells. As anticipated, the PTX-loaded TPGnRH triggered further decrease in cell proliferation and a drastic increase in the number of cells at the G2/M phase (*P*<0.0001). Interestingly, a physical mixture of the PTX and TPGnRH effect on G2/M cell cycle arrest is statistically significant from PTX-loaded TPGnRH nanofibers (*P*<0.05) implying that PTX is uptaken by the cell within the nanofibers and released in intracellular compartments of the cells. Following the effect on proliferation, apoptosis was quantified using Annexin V/PI (Fig.

7e). TPGnRH nanofibers instigated early and late apoptosis on U-87 MG cells (Fig. 7f), and the addition of a PTX-loaded TPGnRH cycle resulted in an increased of apoptotic cells compared to PTX (1 nM) or TPGnRH alone ($P$<0.0001) (Fig. 7e). Taking these results, it is clear that the binding of the novel GnRH analogue to a GPCR triggers signalling cascades leading to an effect on tumour proliferation and apoptosis. PTX entrapped within the TPGnRH nanofibers is, possibly, uptaken within the fibers intracellularly attenuating the cytotoxicity of TPGnRH. In the case of GnRH-R, it has been suggested the coupling of this GPCR to a $G_{\alpha i}$ protein in GBM cells, which inhibits a cAMP-dependent pathway by acting as an inhibitor of the enzyme adenylate cyclase. Intracellular cAMP was quantified using an ELISA kit (Fig. 7g). Both GnRH analogues, goserelin and TPGnRH, counteracted the increase of the cAMP induced by FSK. However, goserelin treatment resulted in no significant effect ($P$>0.05) on tumour cells when added every two days, possibly, due to a low enzymatic stability in U-87 MG cells. TPGnRH fibers counteraction of cAMP was concentration-dependent with nearly complete abolishment of cAMP-dependent signalling at 35 μM (0.51 ± 0.23 pmol $L^{-1}$). PTX-loaded TPGnRH illustrated a similar ability to affect this pathway. Cell uptake studies were also conducted in U-87 MG and SK-OV-3 cells (Fig. 7) to further corroborate the specific antitumour effects of TPGnRH nanofibers via a GPCR. Cellular uptake of TR-TPGnRH nanofibers in U-87 MG cells greatly exceeded the uptake by SK-OV-3 cells at 37 °C with U-87 MG cells showing a 2.45- and 1.85-fold increase in the uptake at 1 and 4 hours of incubation with labelled nanofibers, respectively. Experiments at 4 °C demonstrated that cellular uptake in the U-87 MG cells is energy-dependent with a significant reduction of TR-TPGnRH$^+$ cells ($P$<0.001) (Fig. 7). On the contrary, SK-OV-3 cell uptake was not statistically significant at the different temperatures ($P$<0.05) enlightening the role of GnRH-R in the antitumour effects of TPGnRH.

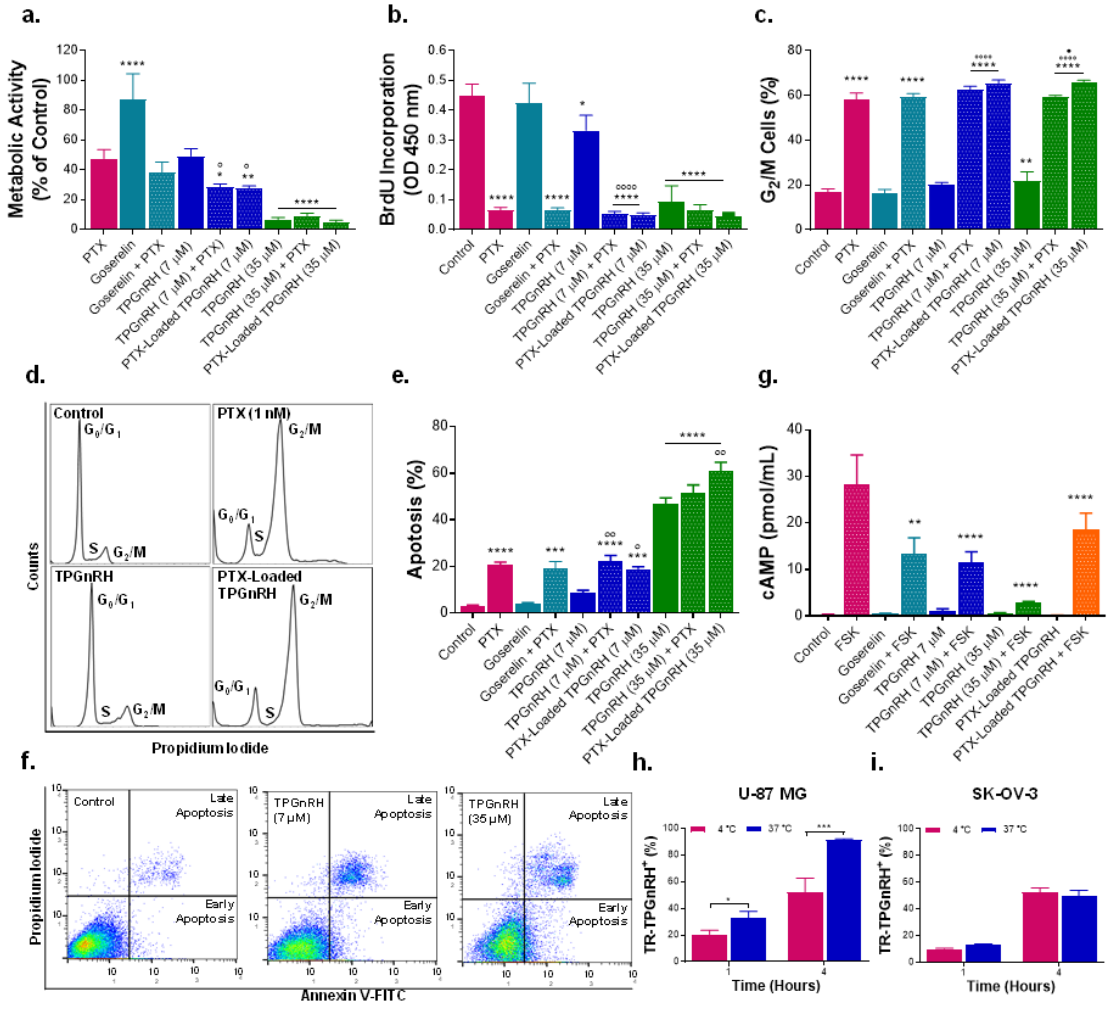

Figure 7. ***In vitro* antitumour effect of TPGnRH nanofibers on GBM**. (a) Metabolic activity of the U-87 MG cells treated with TPGnRH/PTX-loaded TPGnRH during 6 days. Pre-treatment with TPGnRH (two doses) and one dose of PTX-loaded TPGnRH. Mean ± SD (*n*=3 cells, 3 independent experiments). * *P*<0.05, ** *P*<0.01, **** *P*<0.0001 compared to the PTX alone. ° *P*<0.05 compared to TPGnRH (7 μM) (One-Way ANOVA, Tukey's post hoc). (b) Proliferation, (c) percentage of cells at $G_2$/M phase, (d) histograms showing cell cycle arrest at $G_2$/M phase, and (e) apoptosis after a treatment of U-87 MG cells with TPGnRH and PTX-loaded TPGnRH for 6 days. Mean ± SD (*n*=3 cells, 3 independent experiments). * *P*<0.05, ** *P*<0.01, *** *P*<0.001, **** *P*<0.0001 compared to control. ° *P*<0.05, °° *P*<0.01, °°° *P*<0.001, °°°° *P*<0.0001 compared to the TPGnRH alone. • *P*<0.05 comparing the physical mixture to PTX-loaded TPGnRH (One-Way ANOVA, Tukey's post hoc). (f) Dots plots showing apoptosis caused by TPGnRH nanofibers after 6 days of treatment every two days. (g) TPGnRH nanofibers effect on cAMP accumulation on U-87 MG cells. Mean ± SD (*n*=3 cells, 2 independent experiments). ** *P*<0.01, **** *P*<0.0001 compared to control (One-Way ANOVA, Tukey's post hoc). (h) TR-TPGnRH nanofiber uptake by U-87 MG cells. Mean ± SD * *P*<0.05, *** *P*<0.001, comparing uptake at different temperatures (Unpaired Student's *t*-test).

**Milestone 3 (MO3); Antiproliferative effects of peptide nanofibers assessed in low passage GBM lines from biopsies (Dr Lalatsa, Prof Pilkington, Prof Hinterdorfer (Linz, Austria))**

*Expression of GnRH-R in Biopsy-Derived GBM Cells (Table 1)*

Initially, the expression of GnRH-R in the different GBM cell lines was assessed using ELISA (Figure 8, Table 1). The expression of GnRH and GnRH-R was previously demonstrated in the immortalised cell line U-87 MG [4], and thus U-87 MG cells were used as a positive control. Three of the GBM cell lines (SNB-19, UP-029 and SEBTA-023) revealed lower levels of GnRH-R (< 20 ng $mL^{-1}$) comparing to U-87 MG cells. Interestingly, one of the biopsy-derived cell lines, UP-007, displayed similar amount of GnRHR as the positive control (P>0.05). These results suggest that despite the cellular heterogeneity of GBM, GnRHR is identified in a range of immortalised and biopsy-derived cell lines acting as a novel target for GBM.

Table 1 – Details of GBM cell lines SNB-19, UP-007, UP-029 and SEBTA-023.

| Cell line | Sex | Age | Location | Other |
|---|---|---|---|---|
| SNB-19 | Male | 47 | Left Parietal-Occipital Lobe | - |
| UP-007 | Male | 71 | - | Wild-type IDH1 |
| UP-029 | Female | 66 | - | Wild-type IDH1/IDH2 |
| SEBTA-023 | Male | 70 | Left Parietal Lobe | 68.5% MGMT Methylation |

Key**: MGMT, O-6-methylguanine-DNA methyltransferase; IDH, isocitrate dehydrogenase.**

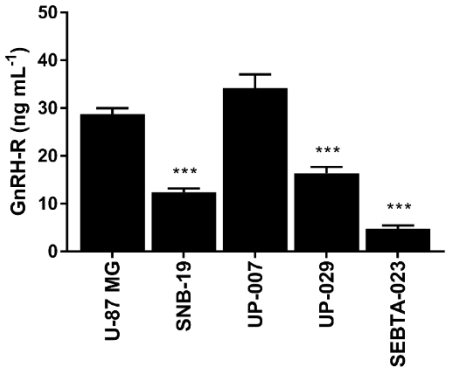


Figure 8 – **GnRHR expression in immortalised and biopsy-derived GBM cells**. Quantification of the GnRHR in immortalised (U-87 MG and SNB-19) and biopsy-derived cell lines (UP-007, UP-029 and SEBTA-023) using a human GnRH-R ELISA. Mean ± SEM (*n*=3). *** *P*<0.001 comparing to the positive control (U-87 MG), One-Way ANOVA with Tukey's post-hoc.

### *Anti-Tumour Effect of the Peptide Nanofibers*

The confirmation of the expression of GnRHR in a range of immortalised and biopsy-derived cell lines encouraged us to explore the effect of the novel TPGnRH nanofibers in GBM. Stock solutions of TPGnRH nanofibers were prepared in PBS above the previously described critical concentration aggregation (135 μM), and GBM cell lines were treated with 3 doses of nanofibers at concentrations ranging 0.25-40 μM for 6 days. After the 6 days, TPGnRH nanofibers significantly reduced cell viability ($P$<0.05) of the four tested GBM cells (SNB-19, UP-007, UP-029, and SEBTA-023) (Figure 9). Figure 9 depicts a dose-response of TPGnRH nanofibers in the tested GBM cell lines with the nanofibers being significantly effective at doses > 5 μM. $IC_{50}$ values for each cell line were calculated (Table 2). Our previous work with U-87 MG cell line, TPGnRH nanofibers revealed an $IC_{50}$ of 10.3 ± 3.5 μM, which is similar to the obtained values for UP-007 (11.8 ± 1.6 μM). SNB-19 and SEBTA-023 revealed slightly higher $IC_{50}$ values (15.7 ± 5.5 and 18.2 ± 3.4 μM, respectively) compared to UP-007 and U-87 MG. These results correlate with the ELISA GNRHR expression data (Figure 8) suggesting that low $IC_{50}$ values are associated with higher expression of GnRHRs in the GBM cells. UP-029 cells revealed a significantly higher $IC_{50}$ ($P$<0.0001) compared to the other three cell lines even though the expression of GnRHR is similar to the immortalised SNB-19 cell line.

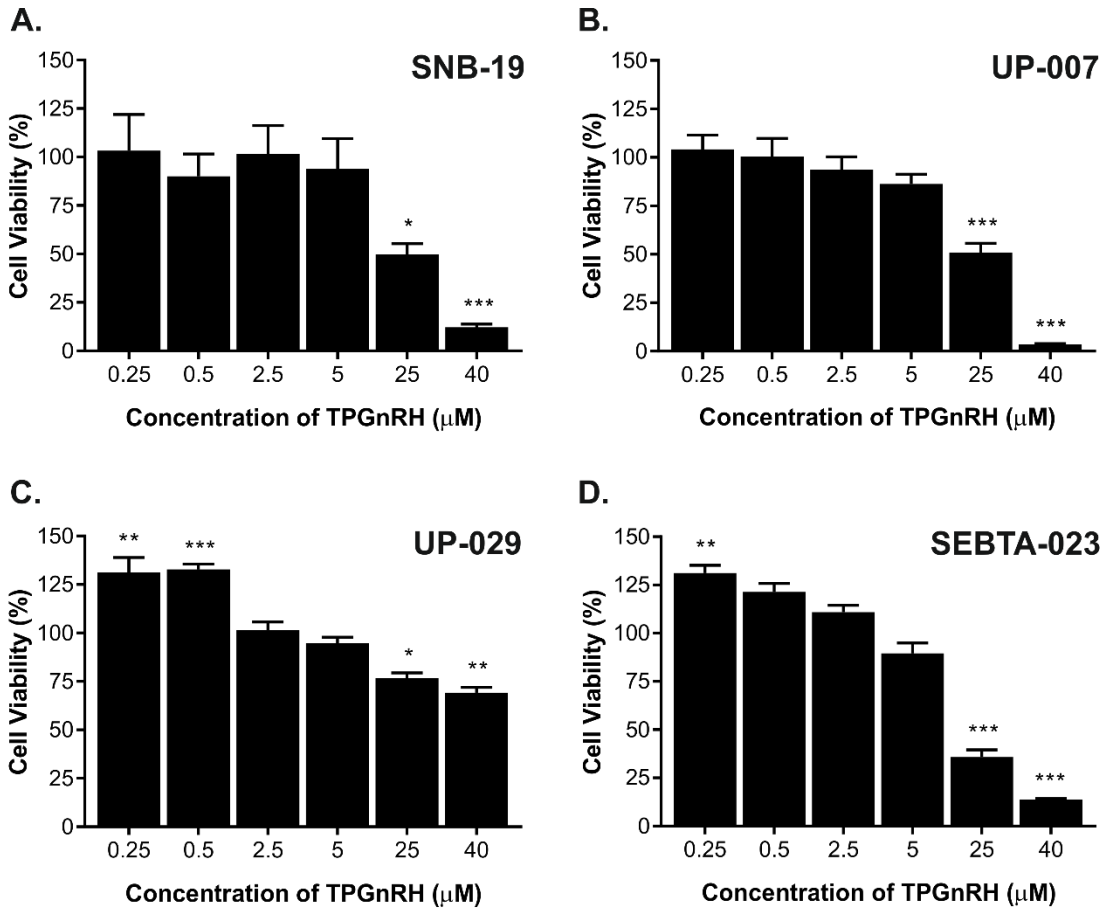


Figure 9 – **Anti-tumour effect of the TPGnRH nanofibers on GBM cells.** (A) SNB-19, (B) UP-007, (C) UP-029, (D) SEBTA-023 cells were treated, every two days, with a range of concentrations of TPGnRH nanofibers (0.25 to 40 μM) for 6 days. Cell viability was assessed at day 6 and expressed as a relative percentage to the control cells (untreated cells). Mean ± SEM (*n*=9). * *P*<0.05, ** *P*<0.01, *** *P*<0.001 comparing to the untreated cells, One-Way ANOVA with Dunnett's post-hoc.

Table 2 – $IC_{50}$ of TPGnRH nanofibers on GBM cells. GBM cells were treated, every two days, with a range of concentrations of TPGnRH nanofibers (0.25 to 40 μM) for 6 days. $IC_{50}$ was calculated at day 6.

| Cell Line | $IC_{50}$ (μM) |
|---|---|
| SNB-19 | 15.7 ± 5.5 |
| UP-007 | 11.8 ± 1.6 |
| UP-029 | 91.5 ± 28.9 |
| SEBTA-023 | 18.2 ± 3.4 |

*Specificity of the Binding of the Peptide Nanofibers to GnRHR*

AFM-based SMFS was carried out to confirm the interactions between the nanofibers and the GnRH-Rs expressed on biopsy-derived GBM cells (UP-007, UP-029, SEBTA-023). For this purpose, the parent Glu-GnRH and TPGnRH nanofibers were covalently attached to amino-functionalised AFM tips via a heterobifunctional cross-linker (NHS-$PEG_{18}$-aldehyde). Using the functionalised tips, hundreds (500-1000) of force distance curves were recorded on living GBM cells. Before the tip touched the cell surface no force is transmitted to the tip, which is reflected by a horizontal zero-force line. After bringing the tip to contact with the cell surface, the tip indented the cell surface and the force is transmitted to the AFM tip in a quasi-linear manner. At this point, the receptor-ligand is formed between the GnRHR and Glu-GnRH/TPGnRH. Subsequently, retracting the tip from the cell surface, the pulling force is gradually loaded in a non-linear manner on the bond of GnRH-R/Glu-GnRH or GnRH-R/TPGnRH and the complex is pulled apart with the tip returning to the rest position. In case of no interaction between GnRHR and the ligands, a horizontal zero-force line is obtained. By analysis of hundreds of force-distance curves, the overall binding probability (i.e. the probability of recording an unbinding events in the force-distance curves) of Glu-GnRH and TPGnRH was calculated for each of the biopsy-derived cell line (Figure 10). TPGnRH displayed a binding probability of 25.37, 9.514 and 13.83% to the GnRH-R in UP-007, UP-029 and SEBTA-023, respectively. UP-007 cell line presented a statistically significant greater binding probability ($P$<0.01), which correlates to the higher expression of GnRHR at the cell surface. Comparing to the parent peptide (Glu-GnRH), TPGnRH nanofibers demonstrated a superior binding to the GnRHRs in all tested GBM cells indicating the potential of these nanostructures to bind to the GnRHR at a greater extent than other GnRH analogues. From the same force-distance curve (retraction speed 1 μm $s^{-1}$), the unbinding force was extrapolated for the GnRH-R/Glu-GnRH and GnRH-R/TPGnRH complexes (Figure 9). Both ligands revealed an unbinding force of ~ 40 pN in the tested GBM cell lines, which implies that the binding occurs at the same binding pocket within the GnRHRs. To further confirm the specificity of the binding to GnRHRs, blocking experiments, in which the receptor sites are masked by the addition of free ligands, were done using a GnRH analogue, goserelin (Figure 11). Goserelin (50 μg $mL^{-1}$), which specifically binds to GnRHRs, was added and allowed to bind for 1 hour at room temperature. After 1 hour incubation, the same cell was analysed with an AFM tip functionalised with TPGnRH nanofibers and the unbinding probability was calculated for each cell line. Addition of goserelin to GBM cell lines resulted in a ~ 2-fold reduction in the unbinding probability of TPGnRH fibers to the GnRH-R establishing the specificity of the binding of the nanofibers (Figure 11).

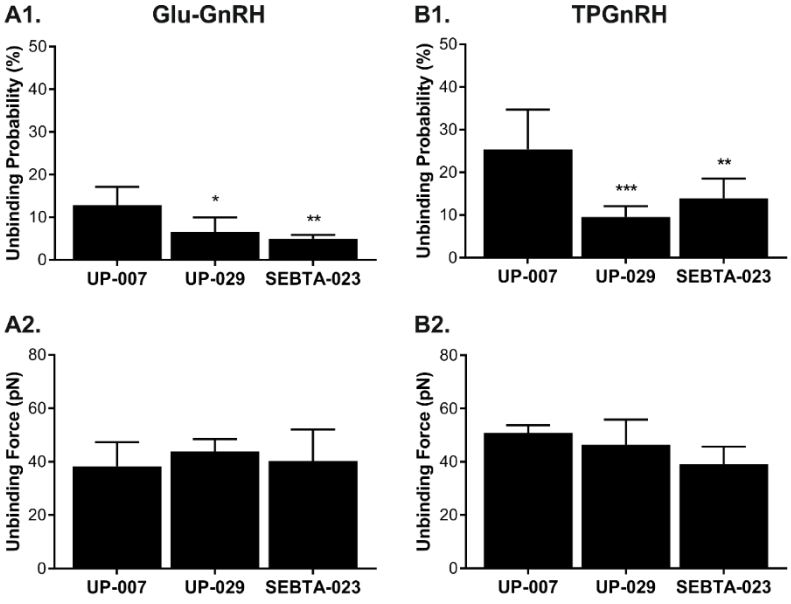

Figure 10 – **Unbinding probability and force of Glu-GnRH and TPGnRH nanofibers to GnRHR in biopsy-derived GBM cells**. (A) Glu-GnRH unbinding probability (A1) and force (A2) to the GnRHR on UP-007, UP-029, and SEBTA-023. (B) TPGnRH nanofibers unbinding probability (B1) and force (B2) to GnRHR on biopsy-derived GBM. Cells were analysed with tips functionalised either with Glu-GnRH or TPGnRH nanofibers at a retraction speed of 1 μm $s^{-1}$. Mean ± SD (*n*=4-14).* *P*<0.05, ** *P*<0.01 comparing to the UP-007 cell line, One-Way ANOVA with Tukey's post-hoc.

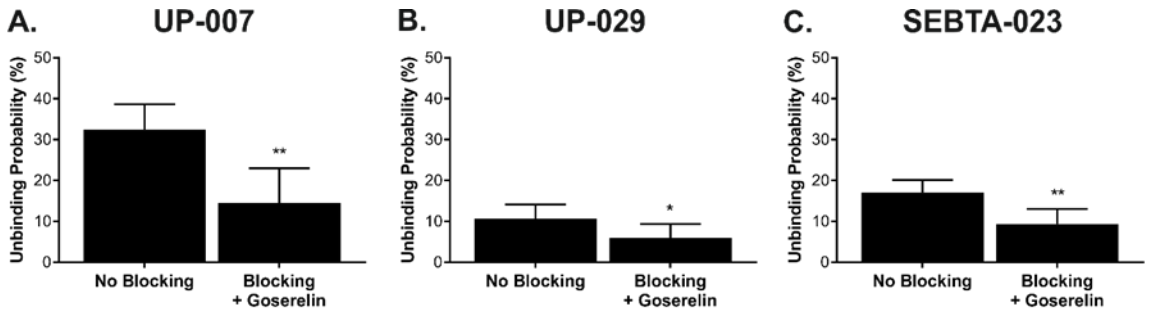


Figure 11 – **Unbinding probability of TPGnRH nanofibers to GnRHR on GBM cells before and after the addition of a GnRH analogue, goserelin**. Unbinding probability of TPGnRH/GnRH-Rs on UP-007 (A), UP-029 (B) and SEBTA-023 (C), before (no blocking) and after (blocking + goserelin) the addition of free goserelin. Retraction speed of 1 μm $s^{-1}$. Mean ± SD (*n*=5-8).* *P*<0.05, ** *P*<0.01 comparing no blocking to a blocking with goserelin, Student's t-test.

*Kinetics of the Binding of the Peptide Nanofibers to GnRHR*

To comprehend the binding of TPGnRH nanofibers to the GnRH-Rs on GBM, SMFS was performed at different loading rates ($10^1$-$10^4$ pN $s^{-1}$). For each loading rate, events were identified on the force-distance curve and the corresponding unbinding force was obtained for each TPGnRH/GnRH-R complex. Afterwards, the logarithm of the loading rate (pN $s^{-1}$) was plotted versus the most probable unbinding force (pN). In these plots, a linearity was found confirming that the measured forces between TPGnRH/GnRH-R are single-molecule interactions. Using Bell-Evans model to fit the SMFS data at different loading rates, the dissociation rate ($k_{off}$) (rate constant for the receptor-ligand dissociation in the absence of applied force) and energy barrier ($x_b$) (distance between the free-energy minimum to the transition state barrier) were extrapolated for the TPGnRH nanofibers (Figure 5). As shown on Figure 5A, TPGnRH nanofibers displayed a $k_{off}$ of 1.23 ± 0.13, 2.03 ± 0.18 and 1.8 ± 0.11 $s^{-1}$ to GnRH-Rs on UP-007, UP-029 and SEBTA-032, respectively. Interestingly, the UP-007 shows a statistically significant $k_{off}$ value (*P*<0.001) comparing to the other two cell lines. This greater $k_{off}$ may be related to an increased time of residence of TPGnRH nanofibers within the GnRH-R pocket on UP-007. Additionally, the UP-007 cell line also showed a statistically significant inferior $x_b$ comparing to UP-029 and SEBTA-023 (*P*<0.001).

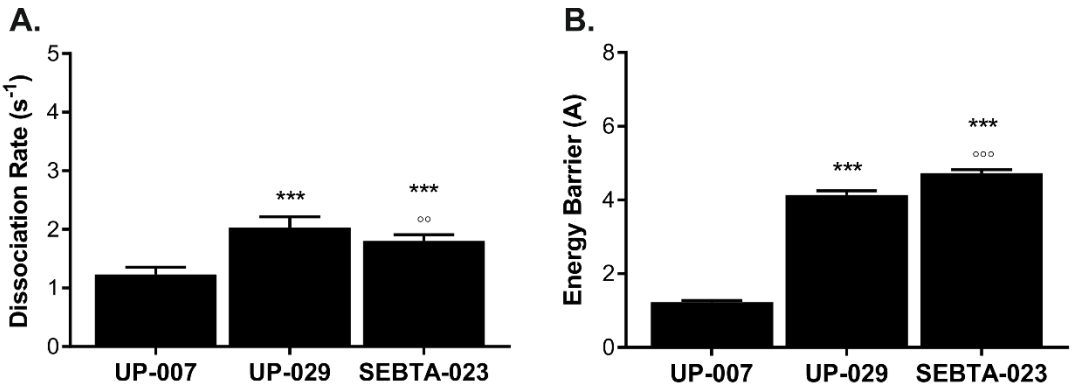


Figure 12 – **Dissociation rate and energy barrier of TPGnRH fibers on the biopsy-derived GBM cell lines**. AFM tips were functionalised with the TPGnRH nanofibers and GBM cells were analysed at a retraction speed of 1 µm $s^{-1}$. Mean ± SD (*n*=5-8). *** *P*<0.001 comparing to UP-007 cells, °°° *P*<0.001 comparing UP-029 versus SEBTA-023, One-Way ANOVA, Tukey's post-hoc test.

Biopsy-derived cell lines were treated with two doses of TPGnRH nanofibers (7, 14 or 35 µM, every two days for 4 days). On day 4, PTX-loaded TPGnRH nanofibers containing 1 nM PTX and 7, 14 or 35 µM of TPGnRH were added and viability was assessed on day 6. The justification for this experimental set up is that the pre-treatment with TPGnRH nanofibers reduces cell viability and one dose of the formulation PTX-loaded TPGnRH is enough to affect the remaining GnRHR- cells (dose-sparing). As shown in Figure 13, the treatment of two biopsy-derived GBM cells with TPGnRH nanofibers (> 7 µM) causes a significant reduction in viability in a dose-dependent manner. When treated with one dose of PTX-loaded TPGnRH, the effects of TPGnRH nanofibers are combined with PTX resulting in a greater decrease in cell viability comparing to TPGnRH alone (P<0.001). Intriguingly, UP-029 cell line showed no response to PTX and thus, no significant effects were observed with the PTX-loaded TPGnRH nanofibers. However, the versatile nature of the TPGnRH nanofibers would possibly allow for the entrapment/encapsulation of cytotoxics that affect UP-029 cell viability and/or metabolism.

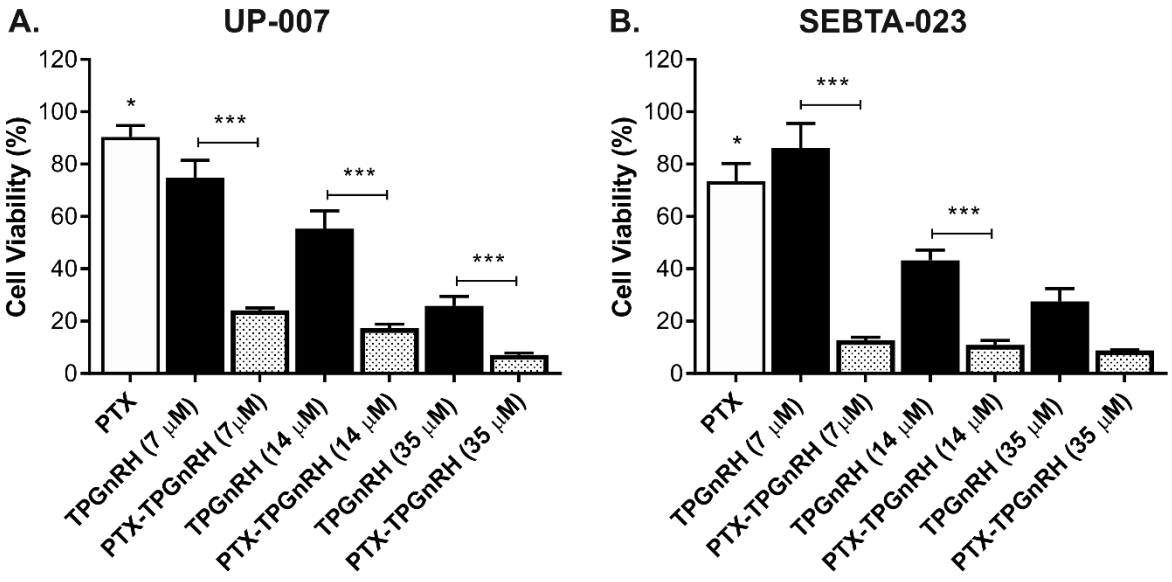


Figure 13 – **Anti-tumour effect of PTX-loaded TPGnRH nanofibers of low passage GBM cells from biopsies.** UP-007 and SEBTA-023 cells were either treated with PTX (1nM), unloaded TPGnRH fibers (7, 14 or 35 µM) or a combination of TPGnRH nanofibers and PTX-loaded TPGnRH (1 nM of PTX and

7, 14 or 35 µM TPGnRH) for 6 days. When treated with PTX-loaded TPGnRH, cells were initially treated with two doses of TPGnRH for 4 days (every two days), and one dose of PTX-loaded TPGnRH. Cell viability assessed on day 6 and expressed as a relative percentage of the control cells (untreated cells). Mean ± SEM (*n*=9). * *P*<0.05, *** *P*<0.001 comparing to the untreated cells or as indicated in the graph. One-Way ANOVA with Tukey's post-hoc.

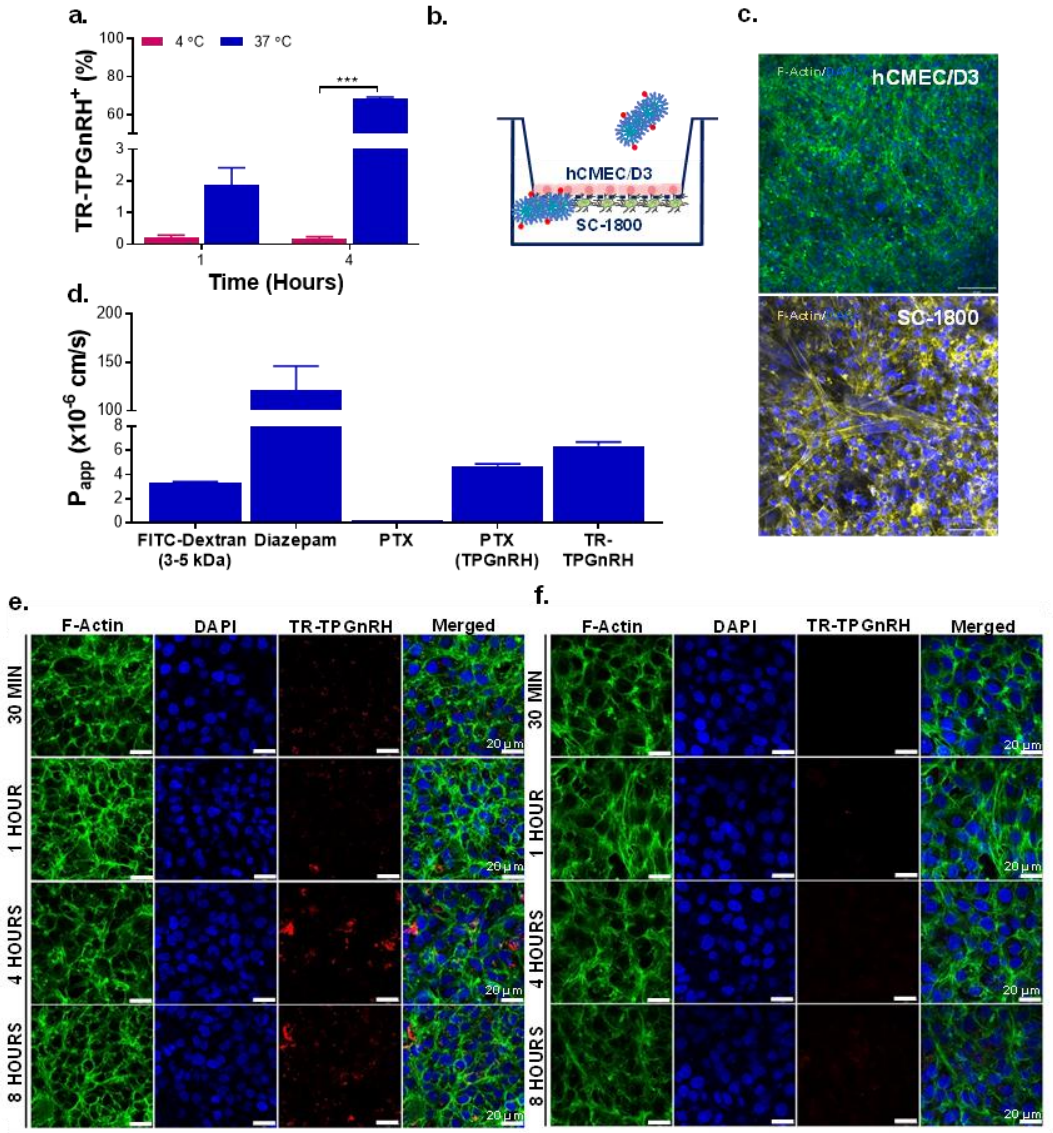


Figure 14. **Permeability of PTX and TPGnRH nanofibers across an all human *in vitro* BBB model**. (a) Endothelial hCMEC/D3 uptake of TR-labelled nanofibers quantified by using flow cytometry after 1 and 4 hours of incubation (4 and 37 °C). Mean ± SD (*n*=3, two independent studies). *** *P*<0.001, comparing TR-TPGnRH$^+$ cells at 4 or 37 °C (Unpaired Student's *t*-test). (b) Schematic illustration of the *in vitro* BBB model using a Transwell system to evaluate the permeation of Texas- Red (TR)-TPGnRH or PAX across endothelial cells (hCMEC/D3) and astrocytes (SC-1800). (c) Morphology of hCMEC/D3 and SC-1800 after 5 days of co-culture. F-actin staining for the cytoskeleton and DAPI s nuclei. Scale bar: 50 µm. (d) Permeability coefficient of FITC-dextran (3-5 kDa), diazepam, PTX, PTX loaded within TPGnRH nanofibers and TR-TPGnRH across the *in vitro* BBB model in luminal to abluminal direction. Mean ± SD (*n*=3, three independent studies). **** *P*<0.0001, comparing to PTX alone (One-Way ANOVA, a Tukey's post-hoc). (e) Confocal images of the permeability of TR-TPGnRH nanofibers across the endothelial cells hCMEC/D3 after 30 minutes, 1, 4 and 8 hours. (f) Confocal images showing accumulation of TR-TPGnRH nanofibers in the astrocytes after 30 minutes, 1, 4 and 8 hours of the addition of the nanofibers to the luminal side of the Transwell. F-actin (green) staining for cell cytoskeleton, DAPI (blue) staining nuclei and Texas Red labelled TPGnRH (TR-TPGnRH) in red representing the nanofibers. Scale bar: 20 µm.

**Milestone 4 (MO4); Permeability studies of nanofibers across an in vitro all human BBB model (Dr Lalatsa)**

The well-established human brain microvascular endothelial cell line (hCMEC/D3) and human cerebral astrocytes (SC-1800) in a contact co-culture as an in vitro BBB model was employed to estimate the permeability of PTX-loaded TPGnRH (Fig. 14b). Initially, the cell uptake of the labelled nanofibers (TR-TPGnRH) was assessed in hCMEC/D3 using non-cytotoxic concentrations of TPGnRH (Fig 14.a). The nanofibers were uptaken by hCMEC/D3 reaching 68.42 ± 0.85% of the TR-TPGnRH+ cells within 1 hour. To understand whether the uptake is an active mechanism, these studies were also carried out at 4 °C. As shown in Fig. 6a, the number of TR-TPGnRH+ cells is greatly reduced either at 1 or 4 hours of incubation (< 0.3% TR-TPGnRH+ cells) suggesting that an energy-dependent mechanism is involved in the permeation of the fibers. Permeability studies using diazepam and FITC-dextran (3-5 kDa) confirmed the ability of the in vitro BBB model to distinguish transcellular and paracellular transport, resulting in the Papp values of 121.29 ± 24.81 and 3.28 ± 0.13 x 10-6 cm $s^{-1}$ for diazepam and FITC-dextran, respectively (Fig. 14d). Free PTX showed a low permeation across the BBB model (Papp 0.19 x 10-6 cm $s^{-1}$) possibly due to active efflux by p-glycoprotein (P-gp), however when loaded within the nanofibers a ~25-fold increase was observed in the Papp (Papp 4.70 ± 0.18 x 10-6 cm $s^{-1}$) of PTX. TR-TPGnRH nanofibers illustrated a Papp 6.0 x 10-6 cm $s^{-1}$ (Fig. 6d). The permeability of TR-TPGnRH nanofibers was also assessed using confocal microscopy. On the luminal side, TR-TPGnRH was uptaken within the cytoplasm of hCMEC/D3 cells within 30 minutes, and as time progressed, a greater accumulation was observed (Fig. 14e). When reaching the SC-1800 cells, TR-TPGnRH permeated across the barrier presenting accumulation within the astrocytes after 4 hours of incubation (Fig. 14f).

***In vivo* pharmacokinetic studies to understand BBB permeability of intraveous administered peptide nanofibers (Dr Lalatsa)**

Apart from completion of all milestones, a further *in vivo* study was undertaken in healthy mice to understand the pharmacokinetic distribution of the peptide nanofibers after administration of an intravenous bolous (35 mg/kg, 5mg/mL in 0.9% sodium chloride) in male 6 weeks old BALB/c mice. Mice were euthanised at 5 and 60 minutes and blood and brain samples were collected. Plasma and brain tissue were homogenised and extracted with ice-cold acetonitrile three times, and the organic layer was dryed centrifugally under vaccuum for 2 and 4 hours respectively prior HPLC analysis. Extraction efficiency was found to be 92.4 ± 2.2% from plasma and 62.3 ± 4.1% from brain tissue. Dose was well tolerated with no signs of acute toxicity in liver, spleen, lung, haemolysis. Fibers demonstrated a long circulation half-life with 6% of the dose remaining in circulation post 60 minutes. Brain levels achieved (0.47 ± 0.01% of the dose) are able to elicity TPGnRH doses that can elicit a therapeutic effect in GBM cells overexpressing the GnRHR. Further studies in orthotopic models are needed to access in vivo efficacy in GBM models.

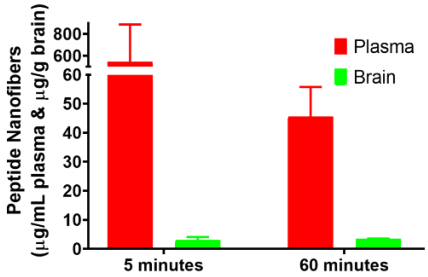


Figure 15. Peptide levels in plasma and brain after intravenous administration of TPGnRH nanofibers (35 mg/kg) after 5 and 60 minutes (n=3).

**Papers/Book Chapters:**

1. Lalatsa, A., Leite, D.M., Figueiredo, M., O'Connor, M. (2017) Chapter 5-5: Nanotechnology in brain targeting: Different nanocarriers, current treatments, merits-demerits and their toxicity profile. In: Kesharwani P. and Gupta U. Ed. Nanotechnology-based Targeted Drug Delivery Systems for Brain Tumours.1st Edition. Elsevier. ISBN: 9780128122181 https://doi.org/10.1016/B978-0-12-812218-1.00005-1
2. Figueiredo, M., Leite, D.M., Lalatsa, A. (2016) Deactivating the ticking bomb of brain diseases with nanomedicines. **Pharmaceutical Technology** 40(9):26-3
3. Leite, DM, Lalatsa, A (2016) Peptide nanomaterials as Targeted Therapies for Glioblastoma. **Journal of Interdisciplinary Nanomedicine**. 1(2):61, DOI: 10.1002/jin2.14.
4. Lalatsa, A. Barbu, E. (2016) Chapter 4. Carbohydrate nanoparticles for brain delivery in K Al-Jamal (ed.), Nanotechnology and the brain. First edition, Elsevier vol. 130, pp 115-53, ISBN: 978-0-12-804636-4
5. Leite, D.M., Barbu, E., Pilkington, G., Lalatsa, A. (2015) Peptide amphiphiles in drug delivery. **Current Topics in Medicinal Chemistry** 15(22):2277-2289
6. Lalatsa, A., Leite, D.M., Pilkington, G. (2015) Nanomedicines and the future of glioma. **Oncology News** 10(2):51-57
7. Lalatsa, A. Leite, D.M. (2014) Single-domain antibodies for brain targeting. **BioPharm** International 27(8):20-26;

**In preparation:**

- Diana M. Leite, Rong Zhu, David Whitley, Chris Read, Peter Cary, Tim Clark, Peter Hinterdorfer, Eugen Barbu, Geoffrey J. Pilkington, Aikaterini Lalatsa. Peptide Nanofibers as an Endocrine Drug Delivery System Targeting G-Protein-Coupled Receptors. Nature Communications (to be submitted)
- Diana M. Leite, Melina F. Figueiredo, Rong Zhu, Peter Hinterdorfer, Eugen Barbu, Geoffrey J. Pilkington, Aikaterini Lalatsa. Understanding the Interaction of Peptide Nanofibers with G-Protein-Coupled Receptors on Glioblastoma Cells Journal of Controlled Release (to be submitted)

**Patent**

Lalatsa, A, Leite DM. Peptide Nanofibers. In preparation for submission April 2018.

**Talks/Conferences:**

1. Lalatsa, A (Oral Presentation) Targeted Peptide Nanofibers for Brain Diseases and Tumours in Controlled Release Delivery (15th Annual SMi Conference), Copthorne Tara Hotel, Kensington, London, 21st March 2018
2. Leite, D.M., Whitley, D., Zhu, R., Barbu, E., Hinterdorfer, P., Pilkington, G., Lalatsa, A. (2017) Peptide nanomaterials as targeted therapy for glioblastoma. UK & Ireland Controlled Release Society Symposium, University of Strathclyde, Glasgow, UK (31st May 2017). Best oral presentation prize.
3. Leite, DM, Zhu, R, Barbu, E, Hinterdorfer, P, Pilkington, GJ, Lalatsa, A (Poster) T7021: Peptide nanofibers as targeted therapies for glioblastoma multiforme in 2015 AAPS Annual Meeting and Exposition 2017 – San Diego Conference Centre, San Diego, USA (14th November 2017). Awarded AAPS Travelship.
4. Leite, DM, Lalatsa, A. (Oral Presentation) Peptide nanomaterials as targeted therapies for glioblastoma in British Society of Nanomedicine Early Career Researchers Meeting, Swansea University, Swansea, 11-12th August 2016. Best oral presentation prize.

5. Lalatsa, A (Oral Presentation) The Nanomedicine Experience in Controlled Release Delivery (14th Annual SMi Conference), Copthorne Tara Hotel, Kensington, London, 3rd April 2017.

**Posters**

1. Leite, D.M., Whitley, D., Zhu, R., Barbu, E., Hinterdorfer, P., Pilkington, G., Lalatsa, A. (2017) Poster 178; Peptide nanomaterials: Targeted therapies for glioblastoma multiforme? American Association for Cancer Research, Washington, US, 2nd April 2017.

2. Leite, D.M., Barbu, E., Pilkington, G., Lalatsa, A. (2015) Peptide nanofibers as a therapy for glioblastoma. Postgraduate Research Student Poster Event. Portsmouth, UK. Runner-up prize for Best Poster Presentation.

**References:**

1. Mazza, M., et al. Nanofiber-based delivery of therapeutic peptides to brain. ACS Nano, 2013. 7(2): p. 1016-1026
2. Lee, O.-S., V. Cho, and G.C. Schatz. Modelling the self-assembly of peptide amphiphiles into fibers using coarse-grained molecular dynamics. Nano Letters, 2012. 12(9): p. 4907-4913.
3. Flanagan, C.A., P. Millar, and N. Illing, Advances in understanding gonadotrophin-releasing hormone receptor structure and ligand interactions. Reviews of Reproduction 1997. 2: p. 113-120.
4. Montagnani Marelli, M. et al. Novel insights into GnRH receptor activity: role in the control of human glioblastoma cell proliferation. Oncology reports 2009. 21: p. 1277-1282.